

http://pubs.acs.org/journal/aesccq Article

# Unexpected Source and Transport of Iron from the Deep Peru Margin

Phoebe J. Lam,\* Maija I. Heller, Paul E. Lerner, James W. Moffett, and Kristen N. Buck



Cite This: ACS Earth Space Chem. 2020, 4, 977-992

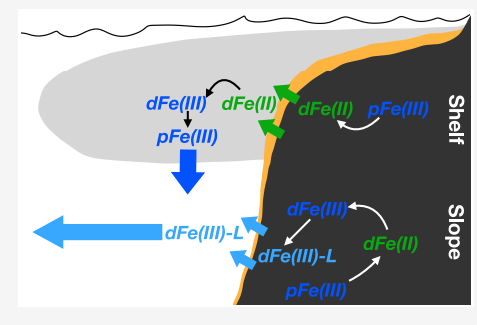


# **ACCESS**

Metrics & More

Article Recommendations

ABSTRACT: Iron is the most important micronutrient in the ocean, but the nature and magnitude of its sources and sinks to the ocean are poorly constrained. Here we assess our understanding of the sources and sinks of iron in margin environments by synthesizing observations from the U.S. GEOTRACES GP16 Eastern Tropical Pacific Zonal Transect (EPZT) cruise near the Peru margin. GP16 observations showed elevated dissolved iron (dFe) concentrations along the margin, but a larger westward plume of dFe at slope depths (1000–3000 m) in oxygenated waters, rather than at shelf depths (100–300 m) in oxygen deficient waters. We examine the potential explanations for this unexpected observation. Multiple tracers from GP16 suggest that sediment resuspension was important at slope depths, which would lead to enhanced benthic flux of dFe above what was previously measured. The difference



in the apparent persistence and penetration of shelf versus slope plumes of dFe into the interior of the ocean likely results from faster removal rates of the shelf dFe compared to slope dFe. The dFe sourced from the shelf was almost entirely in the dFe(II) form, whereas dFe sourced from the slope was almost entirely in the dFe(III) form. Although benthic dFe(II) diffuses into oxygen deficient overlying waters, there is still oxidation of dFe(II), which precipitates to particulate Fe(III). In contrast, the slope plume appears to persist in a stabilized dFe(III) form. We hypothesize that sediment porewaters with moderate organic carbon delivery to sediments and shallow oxygen penetration are especially good sources of persistent dFe to the water column.

KEYWORDS: Benthic flux, sediment resuspension, continental slope, GEOTRACES, dissolution, scavenging

#### ■ INTRODUCTION

Iron is the most important micronutrient in the ocean, limiting productivity in about a third of the ocean. Because of the central importance of iron in limiting productivity, most major climate models have incorporated an iron cycle in their ocean biogeochemical modules. Recently, the Fe Model Intercomparison Project (FeMIP) was conducted to compare the modeled distributions of iron in 13 major iron-containing biogeochemical modules that are used in global general circulation models (GCMs).<sup>2</sup> This exercise showed that most models achieve global mean iron concentrations that are within a factor of 2 of each other and of observations but that the simulated residence times varied by about 2 orders of magnitude, demonstrating that the input and output fluxes are extremely poorly constrained. A recent GEOTRACES synthesis workshop focusing on the fluxes of trace elements and isotopes (TEIs) at the boundaries between the ocean and the land and atmosphere also concluded that many more process studies were needed to understand the processes governing the sources and sinks of TEIs to and from the ocean boundaries: margin,<sup>3</sup> atmospheric deposition,<sup>4,5</sup> hydrothermal,<sup>6</sup> and sediments.

The purpose of this paper is to focus on what we have learned about the sources and sinks of iron at one ocean

boundary, the Peru continental margin, by synthesizing the findings from the near-margin portion of the U.S. GEO-TRACES GP16 Eastern Pacific Zonal Transect held in 2013,8 and placing these results in the context of several decades of ongoing physical, geological, chemical, and biological investigations at the Peru margin. The major margin-related findings of this cruise include the unexpected deep plume of elevated dissolved iron (dFe) centered around 2000 m, apparently emanating from the continental slope, which penetrated further into the interior that any dFe plumes at shelf depths (100-300 m). 9,10 Classic geochemical models of sedimentary sources of Fe fail to predict this, requiring a reassessment of mechanisms governing the sources and sinks of Fe from the margins. 10,11 We assess potential explanations for this observation and speculate on the global importance of deep margins as Fe sources.

Special Issue: Marine Particle Chemistry: Influence on Biogeochemical Cycles and Particle Export

Received: March 9, 2020 Revised: May 23, 2020 Accepted: May 29, 2020 Published: May 29, 2020





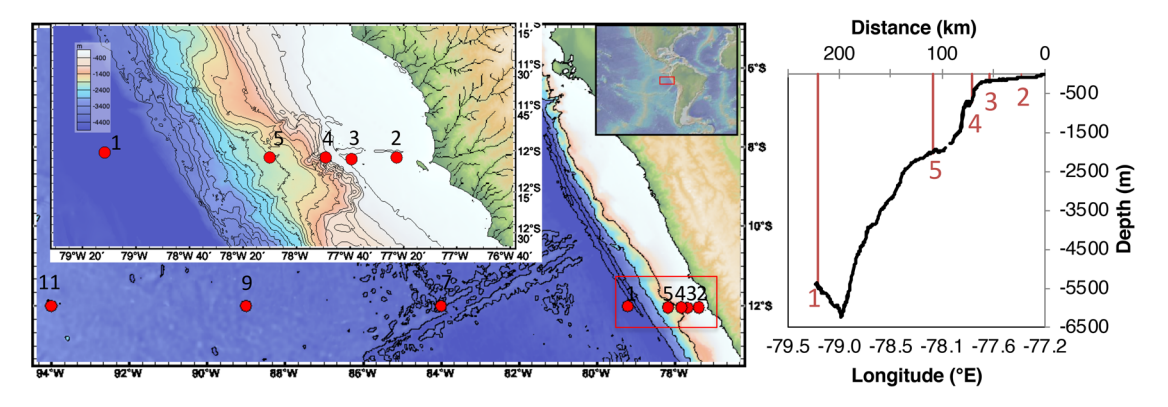


**Figure 1.** Left: Map showing locations of the stations 1–11 (red circles), with inset showing a close-up of the five most coastal stations. Contour lines are 1500 m for the larger map, and 200 m between 0 and 4000 m for the inset. Drainage pathways are indicated in black, but no major rivers are present in this part of the Peruvian coastline. Right: Bathymetric profile of the coastal portion of the GP16 transect. Map and profile created using data from Global Multi Resolution Topography (GMRT) Synthesis<sup>91</sup> extracted in GeoMapApp (http://www.geomapapp.org).

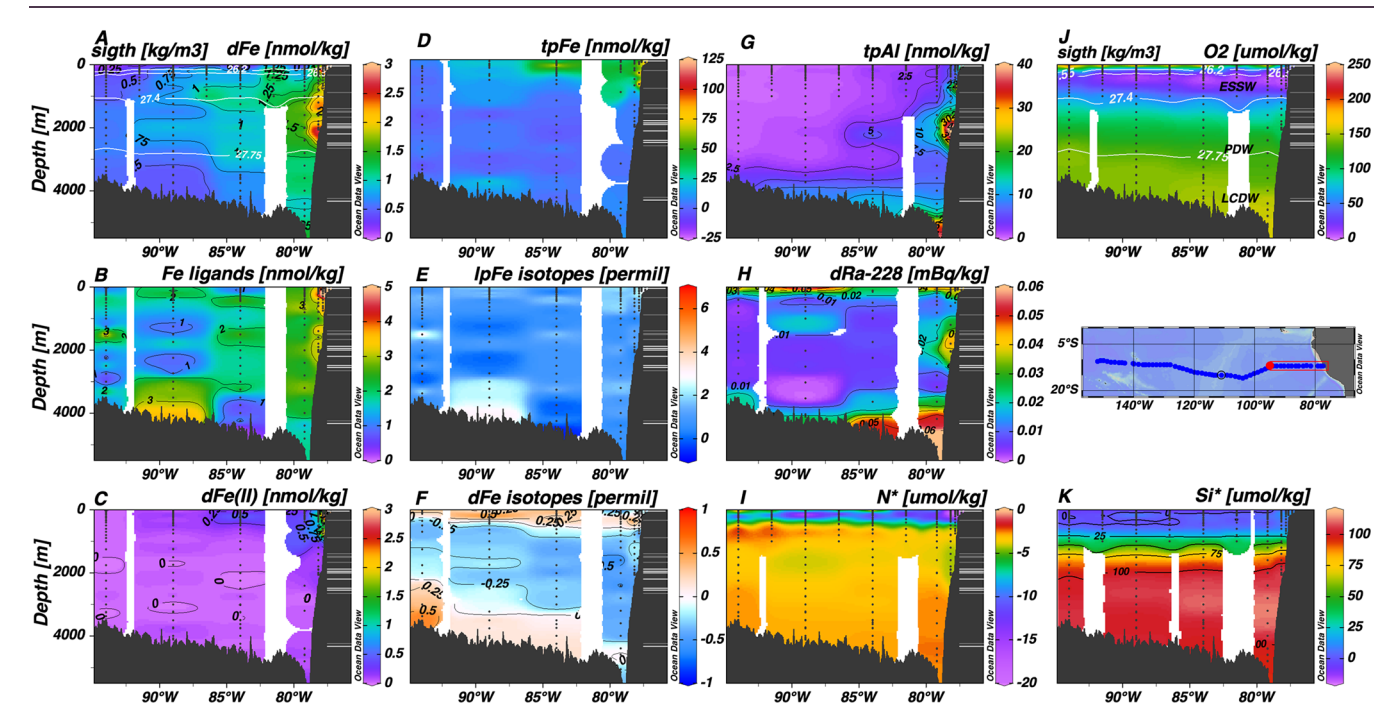


Figure 2. Section plots of multiple chemical and physical parameters along the GP16 transect: (A) dissolved Fe (dFe), (B) the sum of L1 and L2 Fe ligand concentrations (Fe ligands), (C) dissolved Fe(II) (dFe(II)), (D) total particulate Fe (tpFe), (E) leachable particulate Fe isotopic composition in the  $1-51~\mu m$  size fraction (lpFe isotopes), (F) dissolved Fe isotopic composition (dFe isotopes), (G) total particulate Al (tpAl), (H) dissolved  $^{228}$ Ra activity (dRa-228), (I) N-star (N\*), (J) oxygen (O<sub>2</sub>), and (K) Si-star (Si\*). White overlay contours on the dFe and O<sub>2</sub> panels are the potential density surfaces (sigth) used to define the shelf and slope dFe plumes. The main water masses in this region are indicated in panel J: Equatorial Subsurface Water (ESSW), Pacific Deep Water (PDW), and Lower Circumpolar Deep Water (LCDW). All data available from IDP2017<sup>26</sup> and references stated in the text. See Methods for further explanation of variable names. Horizontal lines on the margin show where the slope of the margin is critical for diurnal (white) and semidiurnal (gray) tides.

# **■** HYDROGRAPHIC SETTING

The U.S. GEOTRACES GP16 Eastern Pacific Zonal Transect (EPZT) cruise sailed from Manta, Ecuador to Papeete, French Polynesia on the RV Thomas G. Thompson from 25 October to 20 December 2013. The eastern end of the GP16 transect was in the Peru (Humboldt) Eastern Boundary Upwelling system. The equatorward surface current associated with coastal upwelling is the Peru Coastal Current (PCC). Below this is the Poleward Undercurrent (PUC) that flows along the slope and outer shelf. <sup>12,13</sup>

The central Peru coast  $(7-12^{\circ}S)$ , the region of this investigation, is an extremely arid zone without major fluvial

inputs.<sup>14</sup> This is in contrast to central-south Chile (35–39°S), which experiences strong precipitation and high river discharges that transport large volumes of terrigenous material to the ocean.<sup>14</sup> Overall sedimentation rates thus generally increase southward.

There are year-round upwelling-favorable winds with maximum surface chlorophyll concentrations in austral fall (around March), which is interestingly decoupled from the maximum in upwelling in austral spring (around September). Bottom-moored deep sediment traps (3720 m depth) show POC flux maxima in both austral spring and fall. The wide shelf in northern and central Peru enhances iron supply to upwelling waters at the shelf and thus promotes high

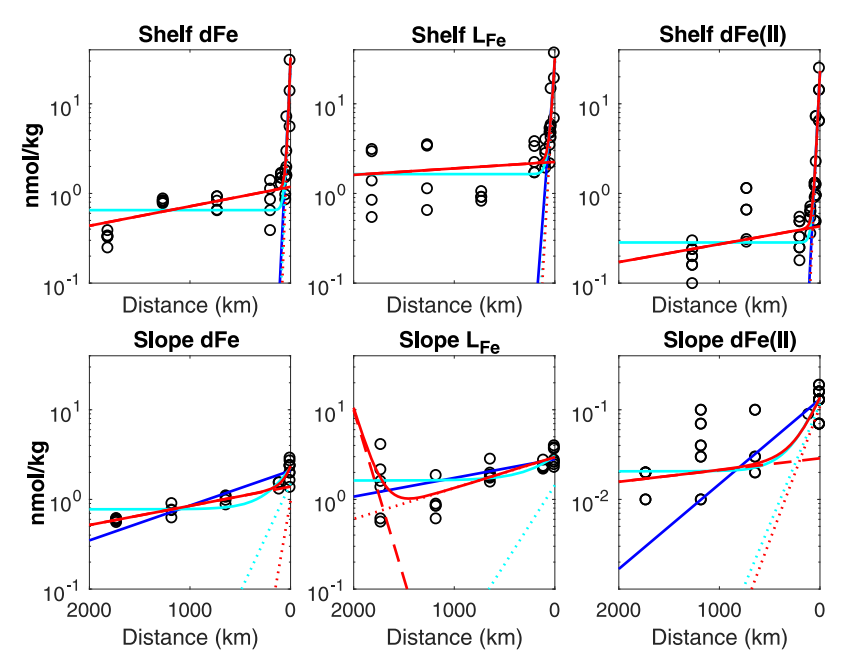


Figure 3. Decreases in concentrations of dFe,  $L_{\rm Fe\prime}$  and dFe(II) in nmol/kg as a function of distance from the coast in km for shelf (top row) and slope (bottom row) depths. Data (circles) are defined by  $\sigma_{\theta} = 26.2 - 26.55$  kg m<sup>-3</sup> for shelf depths and by  $\sigma_{\theta} = 27.4 - 27.75$  kg m<sup>-3</sup> for slope depths. Three exponential-based model fits are in solid colored lines: Model 1 (single exponential) in dark blue; model 2 (single exponential plus a constant) in light blue; model 3 (sum of two exponentials) in red (see text for more details). Dotted and dashed lines in light blue and red are the component exponential functions of models 2 and 3, respectively.

productivity, whereas the narrow shelves of southern Peru and Chile lead to iron limited conditions and thus lower chlorophyll waters.<sup>17</sup> High productivity in the central Peru coast leads to surface sediments that are very high in organic matter (30–35 wt %) compared to further south (15–20 wt %).<sup>14</sup>

Sampling of the first 11 stations closest to the coast (~2000 km) (Figure 1) took place between 29 October and 12 November along 12°S, crossing a relatively wide section of the shelf, after the expected austral spring maxima in upwelling and POC flux.

# NEAR-MARGIN OBSERVATIONS OF FE AND RELATED TRACERS FROM GP16

The major features of dissolved Fe (dFe),9 the isotopic compositions of dissolved Fe $^{10}$  and leachable particulate Fe $^{18}$  dissolved Fe(II) (dFe(II)), $^{19}$  iron binding ligands (L<sub>Fe</sub>), $^{20}$ particulate Fe (pFe),<sup>21–24</sup> particulate aluminum (pAl),<sup>22,23</sup> and <sup>228</sup>Ra<sup>25</sup> have already been described and are also published in the GEOTRACES Intermediate Data Product 2017.<sup>26</sup> Here we focus on the near-margin (stations 1-11) features and interrelationships of these TEIs, all of which are shown in Figure 2. The dFE is highest at the margin with particularly high concentrations at shelf depths (upper few hundred meters) and at midslope depths between 1000 and 3000 m (Figure 2). The shelf dFe plume is largely confined to the 26.2-26.55 kg m<sup>-3</sup> density surfaces in the oxygen deficient zone waters of the Equatorial Subsurface Water water mass.<sup>27</sup> The slope dFe plume is largely confined to the 27.4-27.75 kg m<sup>-3</sup> density surfaces, which are dominantly composed of Pacific Deep Water but also include some Equatorial Pacific Intermediate Water and Antarctic Intermediate Water.<sup>27</sup> The shelf dFe plume, while higher in concentration at its source than the midslope dFe plume, drops off by station 1, ~200 km west of the coast (Figures 1 and 2). In contrast, elevated dFe

concentrations of almost 1 nmol/kg are found more than 1200 km west of the midslope plume (1000-3000 m).

# QUANTITATIVE CHARACTERIZATION OF SHELF AND SLOPE FE PLUMES

To describe the loss of the shelf and midslope dFe plumes penetrating into the interior of the ocean, we assume a first order decay and fit the following exponential models to the dFe concentrations within the shelf plume (defined as  $\sigma_{\theta} = 26.2-26.55 \text{ kg m}^{-3}$ ) and within the slope plume (defined as  $\sigma_{\theta} = 27.4-27.75 \text{ kg m}^{-3}$ ) against the station distance, x

$$C(x) = C_{A} \exp(-k_{A}x) \tag{1}$$

$$C(x) = C_{A} \exp(-k_{A}x) + C_{\text{med}}$$
 (2)

$$C(x) = C_{A} \exp(-k_{A}x) + C_{B} \exp(-k_{B}x)$$
(3)

where C(x) is the dFe concentration as a function of station distance, the parameters  $C_A$  and  $C_B$  are in units of nmol/kg, which we call coastal sources, and the parameters  $k_A$  and  $k_B$  are in units of km<sup>-1</sup>. Model 1 represents a single coastal source of concentration C<sub>A</sub> that decays with distance with an e-folding length scale of  $1/k_{A}$ ; model 2 represents a single coastal source  $(C_A)$  that decays with length scale of  $1/k_A$  on top of a constant, background dissolved Fe (C<sub>med</sub>), defined as the median dFe concentration of stations greater than 500 km from the coast; model 3 represents two coastal sources ( $C_A$  and  $C_B$ ) that decay with length scales  $1/k_{\rm A}$  and  $1/k_{\rm B}$ , respectively. The 500 km cutoff separates the five most coastal stations (Stations 1-5) from the stations further offshore (Figure 1). Model 3 could represent two types of iron sources of different concentrations and length scales of decay. The closest shelf and slope stations (stations 2 and 5, respectively) were defined to be 10 km from their respective margin sources to facilitate comparisons of their source terms.

Table 1. Fit I	Parameters for 1	Three Exponential Models	(eqs 1-3) As Applied to	Table 1. Fit Parameters for Three Exponential Models (eqs 1–3) As Applied to the Decrease in dFe, $L_{F\omega}$ and dFe(II) with Distance <sup>a</sup>	ıd dFe(II) with Die	stance <sup>a</sup>		
	$C_{\mathrm{A}} \; (\mathrm{nmol/kg})$	$k_{\rm A}~({\rm km}^{-1})$	C <sub>med</sub> or C <sub>B</sub> (nmol/kg)	$k_{ m B}~({ m km}^{-1})$	$1/k_{ m A}~({ m km})$	$1/k_{ m B}~({ m km})$	MSE	J
				dFe				
Shelf								
model 1	29 (6)	$5.3 \times 10^{-02} \ (1.3 \times 10^{-02})$			18.9 (4.7)		10.837	$1.5 \times 10^{40}$
model 2	30 (7)	$6.1 \times 10^{-02} \ (1.8 \times 10^{-02})$	0.65 (0.06)		16.3 (4.8)		10.394	35.9
model 3*	32 (11)	$7.0 \times 10^{-02} (3.6 \times 10^{-02})$	1.22 (1.43)	$5.0 \times 10^{-04} \ (1.6 \times 10^{-03})$	14 (7.3)	1,998 (6,244)	10.953	31.4
Slope								
model 1	2.09 (0.12)	$9.0 \times 10^{-04} \ (1.5 \times 10^{-04})$			1,117 (182)		0.130	1.8
model 2	1.50 (0.14)	$5.6 \times 10^{-03} \ (2.3 \times 10^{-03})$	0.78 (0.07)		180 (75)		0.106	1.4
model 3*	0.96 (0.38)	$1.5 \times 10^{-02} (1.9 \times 10^{-02})$	1.39 (0.42)	$4.9 \times 10^{-04} \ (2.7 \times 10^{-04})$	67 (85.3)	2,029 (1,122)	0.100	1.0
				$ m L_{Fe}$				
Shelf								
model 1	29 (5)	$3.4 \times 10^{-02} \ (7.3 \times 10^{-03})$			29.8 (6.5)		20.007	$2.3 \times 10^{26}$
model 2	30 (6)	$4.2 \times 10^{-02} \ (1.0 \times 10^{-02})$	1.64 (0.32)		23.8 (5.6)		17.737	51.9
model 3*	30 (6)	$4.6 \times 10^{-02} \ (1.7 \times 10^{-02})$	2.25 (1.72)	$1.7 \times 10^{-04} \ (7.9 \times 10^{-04})$	22 (7.9)	6028 (28716)	18.789	49.1
Slope								
model 1*	2.81 (0.24)	$4.8 \times 10^{-04} \; (1.4 \times 10^{-04})$			2,081 (588)		0.635	12.3
model 2	1.44 (0.30)	$4.1 \times 10^{-03} (3.1 \times 10^{-03})$	1.63 (0.27)		246.1 (185.8)		0.573	27.7
model 3#	2.96 (0.25)	$7.9 \times 10^{-04} (3.1 \times 10^{-04})$	$3.0 \times 10^{-07} \ (5.8 \times 10^{-05})$	$-8.7 \times 10^{-03} \ (1.1 \times 10^{-01})$	1,260.9 (489.27)	-116 (1457)	0.559	8.0
				dFe(II)				
Shelf								
model 1	22 (3)	$5.1 \times 10^{-02} \ (9.0 \times 10^{-03})$			20 (4)		5.848	$2.3 \times 10^{36}$
model 2*	23 (3)	$5.4 \times 10^{-02} \ (1.0 \times 10^{-02})$	0.28 (0.07)		18 (4)		5.791	48.7
Model 3	23 (4)	$5.6 \times 10^{-02} \ (1.7 \times 10^{-02})$	0.43 (0.84)	$4.6 \times 10^{-04} \ (2.6 \times 10^{-03})$	18 (5)	2176 (12121)	6.015	49.2
Slope								
model 1	0.13 (0.01)	$2.2 \times 10^{-03} (5.1 \times 10^{-04})$			458.8 (107.0)		0.002	4.7
model 2*	0.12 (0.01)	$6.2 \times 10^{-03} (5.3 \times 10^{-03})$	0.02 (0.06)		161 (136)		0.002	1.8
model 3	0.11 (0.03)	$6.9 \times 10^{-03} (9.1 \times 10^{-03})$	0.03 (0.03)	$3.0 \times 10^{-04} \ (9.5 \times 10^{-04})$	144.9 (191.25)	3315 (10424)	0.002	2.5
"Models 1 2 2	nd 2 are a single of	Models 1 2 and 2 are a single exponential a single exponential plus a	of mine a constant and come	constant and sum of two senonantials. Standard server of the fit for each normater is in normathases. MSF and I are the mean	of the fit for each man	anatar is in marantha	buc MSE and	I are the mean

"Models 1, 2, and 3 are a single exponential, a single exponential plus a constant, and sum of two exponentials. Standard error of the fit for each parameter is in parentheses. MSE and J are the mean square error and cost function (eq 4), respectively. Lower values indicate better fits. \*indicates the best fit as assessed by J. #fit is nonsensical (see Figure 3).

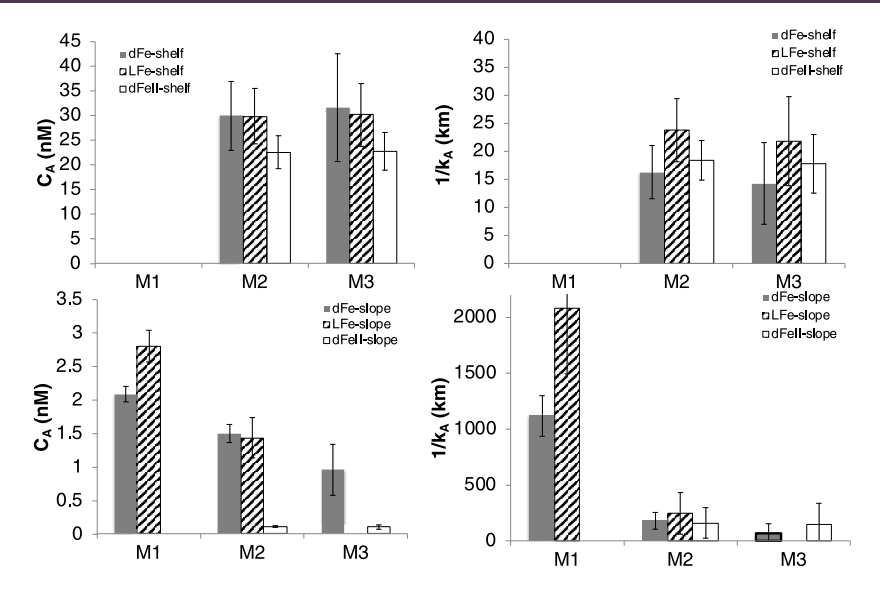


Figure 4. Fit parameters  $C_A$  (source concentration, left panels) and  $1/k_A$  (e-folding length scale, right panels) for the short-lived pool of dFe (solid),  $L_{\rm Fe}$  (hatched), and dFe(II) (open) for the shelf (top two panels) and the slope (bottom two panels) for three exponential models (M1, M2, M3, see text). Models that do not fit the offshore values (M1 on shelf for all parameters, M1 on slope for dFeII) or are nonsensical (M3 on slope for  $L_{\rm Fe}$ ) are not plotted. Error bars are one standard error for the parameter estimate from the nlinfit algorithm in Matlab.

In a typical assessment of the goodness of fit such as the mean square error (MSE), large values are more influential than small values, so a model that minimizes MSE optimizes the fit near the coast, where dFe is high. In order to find a model that optimizes the fit to all data, including the low concentrations offshore, we seek to estimate the parameters of models 1, 2, and 3 that are found at the minimum of the objective function, *J* 

$$J = \sum_{i} \frac{(y_{\text{obs},i} - y_{\text{model},i})^{2}}{y_{\text{model},i}}$$
(4)

where  $y_{\text{obs},i}$  is the observed value of dFe(x) at location i, and  $y_{\text{model},i}$  is the corresponding model. In eq 4, the sum of the squared deviations are normalized by the model values to limit the strong influence of the observed large dFe(x) concentrations on the solution. The best fit was found using Matlab's nonlinear regression algorithm nlinfit. Note that this statistic blows up if the model value is very small compared to the deviation.

A single exponential (model 1) was not able to capture the observed rapid decrease in dFe near the coast, especially for the shelf plume. For both shelf and slope plumes, the best fit was from the sum of two exponentials (model 3) (Figure 3, Table 1), suggesting a strong coastal source with short length scale of decay, and a weaker coastal source with a long length scale of decay. The shelf plume has a short-lived Fe pool with a strong coastal source ( $C_{A,shelf} = 32 \text{ nM}$ ) and short length scale  $(1/k_{\text{A,shelf}} = 14 \text{ km})$  and a long-lived Fe pool with a weaker coastal source ( $C_{B,\text{shelf}} = 1.2 \text{ nM}$ ) and long length scale (1/  $k_{\rm B,shelf}$  = 1998 km). The slope plume has a short-lived pool (1/  $k_{A,\text{slope}} = 67 \text{ km}$ ) with a weak source ( $C_{A,\text{slope}} = 0.96 \text{ nM}$ ) and a slightly stronger long-lived pool ( $C_{\text{B,slope}} = 1.4 \text{ nM}, 1/k_{\text{B,slope}} =$ 2029 km). The length scale of the short-lived Fe pool in the shelf plume is comparable to that found for surface dFe off of Monterey Bay, California of 16 km.<sup>28</sup> In contrast, the length scales of both Fe pools in the slope plume are shorter than the 5000 km length scale for dFe at 1000 m in a transect from central California to the open Pacific.

The longer-lived Fe pools for the shelf and slope plumes have e-folding lengths of about 2000 km and similar source strengths (1.2–1.5 nM), suggesting that they may be similar. In contrast, the shorter-lived Fe pools for the shelf and slope have quite different source strengths ( $\sim$ 30 nM vs  $\sim$ 1 nM) and length scales (14 km vs 67 km), suggesting that they have different sources and speciations that affect their susceptibilities to scavenging.

We assessed the behaviors of the measured species of dFe, dFe(II), and the L1 and L2 classes of Fe-binding ligands ( $L_{\rm Fe}$ ) by fitting the same three exponential models to see whether this could reveal the speciations of the short-lived shelf and slope Fe pools (Figure 3, Table 1). The source concentrations,  $C_{\rm A}$ , and length scales,  $1/k_{\rm A}$ , of  $L_{\rm Fe}$  and dFe(II) in the shelf plume are the same as for dFe within error (Figure 4, Table 1).

For the slope plume, it is clear that dFe(II) has a source concentration that is too small for all models, and  $L_{\rm Fe}$  has a length scale that is too long for models 1 and 3. However, source concentrations and length scales for  $L_{\rm Fe}$  are consistent with those of dFe in the model 2 fit.

The fits to the Fe species thus suggest that the short-lived shelf plume is dominantly dFe(II) and/or ligand-bound Fe, whereas the short-lived slope plume is composed of ligand-bound Fe. The fit results are consistent with the broad distributions, which show that dFe(II) accounted for all of the dFe in the samples taken closest to the sediment at shelf depths, <sup>19,21</sup> and FeL concentrations always exceeded dFe<sup>20</sup> (Figure 2). Note that these Fe species measurements are not necessarily mutually exclusive, since ligand-bound Fe can comprise Fe in the Fe(II) form and may also comprise Fe in the colloidal form.<sup>29</sup>

# SOURCES, SINKS, AND TRANSPORT OF IRON AT THE PERU MARGIN

In this section, we systematically examine all reasonable explanations for the observation of a slope source of ligand-bound iron that penetrates more deeply into the interior than a shelf source that is in the dFe(II) form and/or ligand-bound. Differences in dFe concentrations at shelf and slope depths

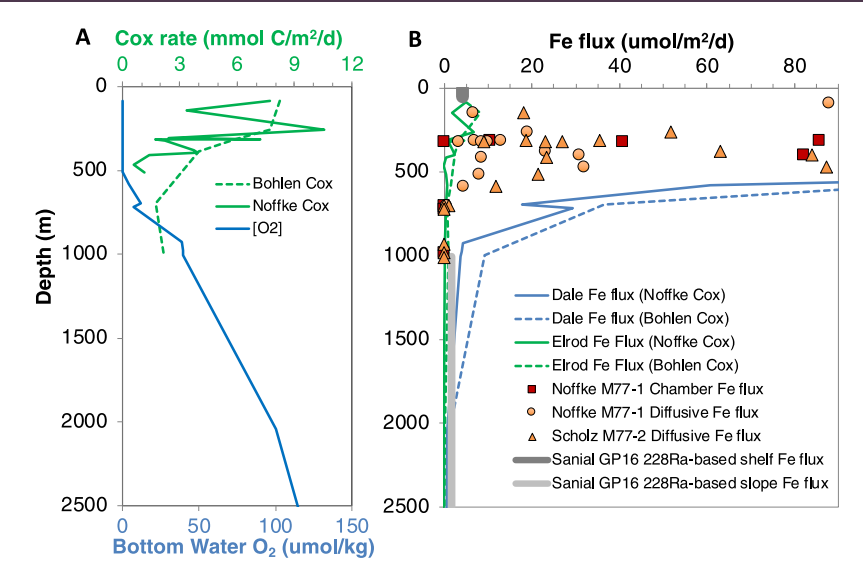


Figure 5. Sedimentary fluxes and concentrations. (A) Measured sedimentary carbon oxidation  $(C_{ox})$  rates (solid green; <sup>102</sup> dashed green <sup>34</sup>) and bottom water oxygen (bottom  $O_2$ ) concentrations (solid blue<sup>34</sup>). (B) Measured and predicted benthic Fe flux at Peru margin; symbols indicate measurements by benthic chamber (red<sup>34</sup>) or from porewater profiles (orange; <sup>34,35</sup> solid and dashed green lines are calculated using the  $C_{ox}$  based model<sup>32</sup> using the Noffke <sup>102</sup> and Bohlen<sup>34</sup>  $C_{ox}$  rate measurements, respectively; solid and dashed blue lines are calculated using the combined  $C_{ox}$  and bottom  $O_2$  model, <sup>33</sup> using  $C_{ox}$  and bottom  $O_2$  measurements of Noffke <sup>102</sup> and Bohlen, <sup>34</sup> respectively; thick dark and light gray vertical lines are shelf and slope Fe fluxes, respectively, estimated based on <sup>228</sup>Ra distributions. <sup>25</sup>

must be attributed to some combination of the following processes: (1) differences in source of dFe, which is defined here as the mobilization of Fe from the particulate to the dissolved phase, either from sediments or from sinking particles; (2) differences in sink strength, which is the conversion of dissolved Fe into particulate Fe through sorption, precipitation, or uptake; (3) differences in circulation, which affects the transport of dFe away from its source; and (4) differences in the mechanisms mobilizing Fe from sediments.

**Differences in Source of dFe.** The two possible sources of dFe are a horizontal source from the margin or a vertical source from the conversion to dFe from sinking particles. The margin source could be a direct source of dFe from sediment porewaters or the conversion to dFe from pFe in resuspended margin particles.

Horizontal Source of Iron from the Margin. Large benthic fluxes of iron result from reductive processes in the sediments, where reduction of sedimentary Fe(III) (oxyhydr)oxides to dFe(II) is coupled to the oxidation of organic carbon to  $\rm CO_2$  when other, more favorable electron acceptors such as  $\rm O_2$ ,  $\rm NO_3^-$ , and  $\rm MnO_2$  are depleted. Measured benthic iron flux typically increases as a function of decreasing bottom water oxygen concentrations and/or increasing sedimentary POC oxidation rate.  $\rm ^{31-33}$ 

Fe flux has been estimated from Peru margin sediments using benthic flux chambers and porewater profiles  $^{34,35}$  and generally shows the highest fluxes (up to 865  $\mu \rm mol/m^2/d$ ) in the sediments that intersect the OMZ (~50–500 m), although with high variability (Figure 5). A model of benthic flux relying only on sedimentary POC oxidation rate  $^{32}$  tends to underestimate measurements, where a model that uses both bottom water oxygen and sedimentary POC oxidation rate  $^{33}$  overestimates measurements. Measurement of dFe(II) in benthic flux chambers  $^{34}$  and in porewater profiles  $^{34,35}$  confirms that reductive dissolution of sedimentary Fe is the mechanism that leads to high near-bottom dFe at shelf depths, consistent with

GP16 measurements of dFe(II) in the water column (Figures 2-4).<sup>19</sup>

As discussed above, the distribution of the shelf Fe plume was similar to the distributions of dFe(II) and Fe-binding ligands (Figures 2–4). Fe(II) is several orders of magnitude more soluble in seawater than Fe(III)<sup>36</sup> and so does not need a stabilization mechanism such as organic complexation or colloids to protect against precipitation. That said, several studies indicate that iron-binding ligands may be involved in the sedimentary reduction of Fe and may explain the similarities in distribution of shelf dFe and Fe-binding ligands.

It has been shown that Shewanella putrefaciens, a facultative marine anaerobe that has the ability to reduce iron and manganese, produces a strong Fe(III)-binding ligand that can solubilize solid phase Fe (oxyhydr)oxides prior to reduction.<sup>3</sup> These authors suggest that dissolved ligand-bound Fe(III) is more easily reduced than solid phase Fe(III) and is thus a strategy to facilitate the use of solid phase Fe (oxyhydr)oxides as electron acceptors to oxidize organic carbon. In later work, this group postulated that the soluble organic-Fe(III) complexes could also be produced by the oxidation of organic-Fe(II) complexes by Fe(III) (oxyhydr)oxides. 38,39 The Peru margin site receives a large supply of labile particulate organic matter from sinking particles, which may provide a source of Fe(II)- and Fe(III)-binding ligands upon remineralization in the sediments. 40-42 The existence of ligands that bound Fe(II) emanating from porewaters were hypothesized to explain much slower Fe(II) oxidation rates in oxygenated bottom waters overlying Celtic Sea sediments than predicted from theoretical rate models.<sup>43</sup> In the Peruvian ODZ, where the main oxidants for Fe(II),  $O_2$  and  $H_2O_2$ , are extremely low and therefore Fe(II) oxidation rates are greatly reduced, the slow oxidation rates of dFe(II) could allow time for formation of ligand complexes<sup>44</sup> that may further retard the

For Peru margin slope sediments below 500 m water depth, where near bottom O<sub>2</sub> concentrations increase to above a few

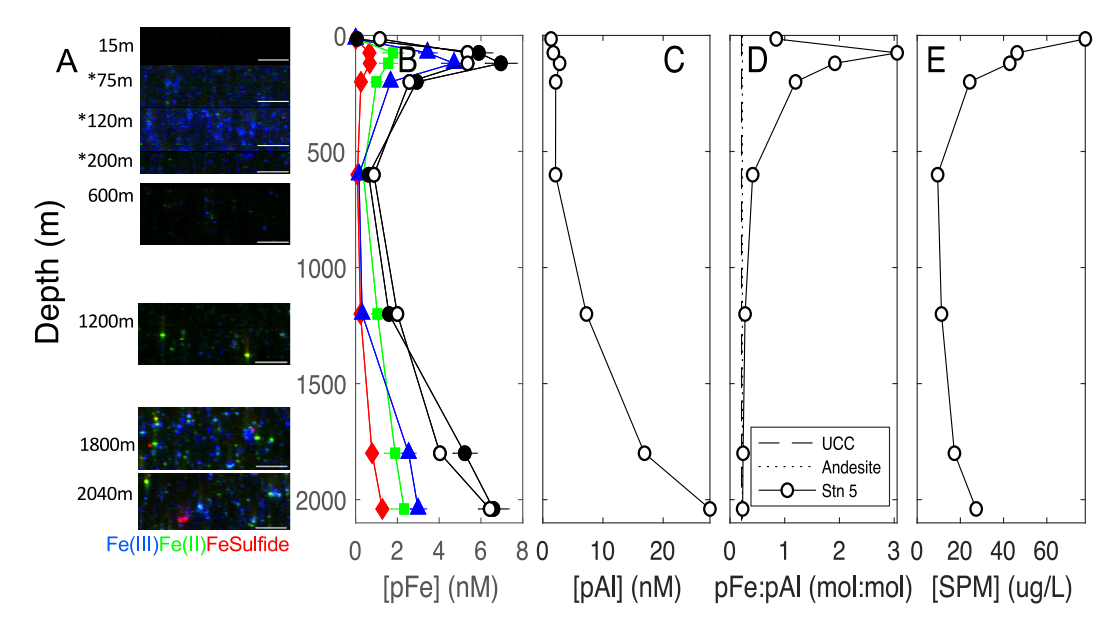


Figure 6. Depth profiles from Stn 5 at  $78.2^{\circ}W$  on the Peru slope (A) of chemical species maps showing the micron-scale distributions of pFe species, (B) quantification of Fe species from A (colors) and total Fe (black, filled and open), (C) total pAl, (D) the molar pFe/pAl ratio, and (E) suspended particulate mass (SPM). Open circles in panels B–D are concentrations determined by ICP-MS. Filled symbols in panel B are concentrations determined by synchrotron uXRF and chemical species mapping with Fe(III) species in blue (triangles), Fe(II) species in green (squares), and Fe sulfide species in red (diamonds). Scale bars in panel A are  $100 \ \mu m$ ; \* indicates a sample in the ODZ; intensities of colors are adjusted so that they are comparable between maps. All data in these panels are from 0.8 to 51  $\mu m$  particles collected by in situ filtration.

micromolar, benthic Fe flux was not measurable using benthic flux chambers or modeling of pore water profiles<sup>34,35</sup> 5). As these methods are best for estimating diffusive fluxes from porewaters, they likely underestimate the true benthic Fe flux from slope sediments as they may not include physical or biological sediment mixing events that would increase flux. A recent study of Black Sea sediments found high benthic Fe flux (360  $\mu$ mol/m<sup>2</sup>/d) despite bottom water oxygen concentrations >200 µmol/kg and elevated porewater dFe(II) more than 2 cm from the sediment-water interface. 45 This study found that bioirrigation was a critical mechanism to enhance benthic Fe flux beyond what is estimated from diffusive processes. In the Peru margin between 500 and 1000 m, elevated dissolved Fe(II) concentrations were found only 1-2 cm below the sediment-water interface. 34,35,46 There are no direct measurements of flux or bioturbation at 2000 m on the Peru margin; however, even if the high dFe(II) were further below the sediment-water interface, previous work has shown that the upper 8-9 cm of sediment at 1210 m on the Peru margin was bioturbated with high concentrations of meiofauna and macrofauna, 47 so there is ample opportunity for bioturbation-induced enhancement of benthic Fe flux from the slope beyond those estimated by benthic flux chambers and pore water profiles. Physical mechanisms to enhance benthic Fe flux are also likely important, which we discuss in a later section.

Several tracers suggest at least some direct influence of reducing porewaters in the water column at slope depths. First, while the majority of the dFe in the water column at slope depths is in the Fe(III) form (Figure 2), as expected for oxygenated waters, dFe(II) at Station 5 (78.2°W) is nonetheless elevated above background ( $\sim$ 0.1 nM) at all depths, well above the 0.014 nM detection limit, <sup>19</sup> even in oxygenated waters. Although dFe(II) is a small percentage ( $\sim$ 5%) of total dFe at slope depths, its presence in oxygenated waters suggests

a relatively constant source from sediments. The rate law for the oxidation kinetics of Fe(II) in seawater is given by 48

$$\frac{-\mathrm{d}[\mathrm{Fe}(II)]}{\mathrm{d}t} = k[\mathrm{Fe}(II)][\mathrm{O}_2][\mathrm{OH}^-]^2$$

where the overall rate constant, k, was empirically determined to be

$$\log k = \log k_0 - 3.29I^{1/2} + 1.52I$$

and

$$\log k_0 = \frac{21.56 - 1545}{T}$$

where T is the temperature in K and I is the ionic strength, which can be calculated from salinity.

For near-bottom waters around 2000 m with T = 2.2 °C, I = 0.715 (S = 34.65),  $[O_2]$  = 103  $\mu$ mol/kg, and pH = 7.73, <sup>49</sup> the Fe(II) oxidation half-life is 20.8 h, long enough to allow a small accumulation of dFe(II) even without ligand stabilization but short enough that it would have to be continually supplied in order to measure it.

Second, there is a negative N\* anomaly adjacent to Station 5 waters between 1000 and 2000 m (Figure 2), suggesting the influence of denitrification. Since dissolved oxygen concentrations at >50  $\mu$ mol/kg are well above the threshold for water column denitrification, this suggests an influence from reducing sediment porewaters. Unlike the dFe(II) signal, however, the negative N\* anomaly is stable and could have been transported from elsewhere.

Third, while the light isotopic composition of dFe at slope depths (Figure 2) was used as an argument for the origin of this dFe plume from dissolution of light pFe from sinking particles, <sup>10</sup> it could also be evidence of the influence of reductive porewaters in adjacent slope sediments. <sup>31,43,50</sup>

As argued above, reductive dissolution processes are likely to be important as a source of Fe from Peru slope sediments, but attention has also been increasingly paid to nonreductive dissolution, which is the dissolution of sediments in oxidizing conditions. Evidence from several isotope systems, including Fe isotopes, support the importance of nonreductive dissolution of aluminosilicate sediments in seawater<sup>51–54</sup> potentially from ligand-mediated and/or microbial dissolution processes. 55,56 Long-term (~1 year) dissolution experiments of several types of sediments from the Kerguelen Plateau in oxygenated seawater showed that sediments rich in biogenic Si released more dissolved iron than basalt-rich or calcite-rich sediments, both in absolute amounts and also as a percentage of the starting particulate Fe concentrations.<sup>57</sup> Biogenic Si is everywhere undersaturated in the water column, so its dissolution should contribute structurally incorporated<sup>58</sup> and/or adsorbed Fe.

Although we do not have direct measurements of the composition of surface sediments around 2000 m, particles in a nepheloid layer in bottom waters at 35 m above the sedimentwater interface at ~2000 m at Station 5 are a reasonable proxy. These nepheloid particles were mainly composed of lithogenic particles (34% weight fraction), biogenic silica (29%), and particulate organic matter (26%).<sup>59</sup> Particles in the nepheloid layer had an Fe/Al ratio of 0.23 mol/mol (Figure 6D), similar to upper continental crust average of 0.21 mol/mol, the Andesite rock average (0.23 mol/mol), and slightly above the 0.19 mol/mol found in surface sediments measured at 2025 m about 100 km north of our station.<sup>35</sup> This is in contrast to suspended particles at OMZ depths, which had Fe/Al far in excess of crustal material (Figure 6D). Synchrotron chemical species mapping and X-ray absorption spectroscopy showed that the high Fe/Al pFe in the OMZ was primarily composed of Fe oxyhydroxides.<sup>21</sup> In contrast, Fe-rich particles at slope depths were minerologically more diverse with a mixture of Fe(II)-, Fe(III)- and Fe-sulfide bearing minerals (Figure 6A). X-ray absorption near-edge spectroscopy showed that for samples below 1000 m, Fe(III) hotspots included clays such as Illite and some Fe oxyhydroxides, Fe(II) hotspots were mainly silicates such as biotite, and Fe sulfide hotspots were pyrite. Since clays, silicates such as biotite, and pyrite cannot form in this water column, their presence indicates resuspension and transport from sediments.

Given the high opal concentration in near-bottom particles, dissolution of biogenic Si from Peru slope sediments may be a source of dFe. Indeed, there is a slight shoaling of the Si\* isolines at the margin around 2000 m, consistent with the dissolution of biogenic Si in near-bottom waters at slope depths at the margin (Figure 2). The slow, nonreductive dissolution of lithogenic Fe may be a potential additional source of dFe at slope depths, but this is more likely to be important in the ocean interior. Rates of nonreductive dissolution of lithogenic Fe would have to be faster than the enhanced scavenging rates from increased particle concentration in order to act as a net source of dFe but measured rates of nonreductive dissolution are wuite slow.<sup>57</sup> Further, mesocosm<sup>60</sup> and modeling<sup>61,62</sup> experiments have shown that the addition of mineral dust frequently decreases dFe concentrations because of enhanced scavenging by the high particle concentrations.

However, the slow dissolution of lithogenic Fe is precisely the characteristic that may explain why relatively insoluble Febearing sedimentary particles may be particularly important as a source of dFe into the deep interior ocean: coastal sources of dFe are scavenged and removed before reaching the interior, but since overall particle concentrations are greatly reduced in the interior the slow lithogenic dissolution rate may be able to compete with the even slower scavenging rate in the interior and act as a net source. On the GP16 transect, pAl concentrations, indicative of lithogenic particles, are elevated above background at 2000 m to 89°W and possibly further (Figure 2), more than 1200 km from the margin, potentially providing a slow release source of dFe into the interior.

Overall, the speciation of the dissolved and particulate phases of Fe suggests that the slope Fe plume has characteristics consistent with a source of Fe from the slope sediments that is primarily ligand-stabilized dFe(III) derived from partial oxidation of reduced porewater dFe(II), a small contribution of dFe(II) directly from porewaters, and potentially from the dissolution of Fe-containing biogenic silica. Further into the interior, the plume may be sustained by the persistence of stabilized dFe from pore waters and potentially the nonreductive liberation of dFe from the slow dissolution of resuspended lithogenic particles.

Remineralization or Desorption Input from Sinking Particles. The source of the slope dFe plume was postulated to be from the remineralization, desorption, and/or dissolution of Fe from sinking particles that were derived from shelf depths. 10 This hypothesis was motivated by the observation of light (negative) Fe isotopes in the dissolved phase in the slope plume (Figure 2). Since light Fe isotopes are a marker of reductive dissolution, which would be expected in the oxygendeficient shelf depths but not in the oxygenated slope depths, John et al. argued that the light Fe isotopes in the slope plume were derived from the regeneration of isotopically light Fe from sinking particles that originated in oxygen-deficient shelf waters. Their hypothesis was supported by a modeling exercise in which they allowed for an input of Fe from reducing sediments at shelf depths and allowed for reversible scavenging from sinking particles. A partition coefficient,  $K_{dv}$  of 0.1 reproduced observations, requiring an exchangeable particulate Fe concentration of 10-100 pM, which John et al. deemed was plausible given ligand leachable particulate iron concentrations of about 1 nM.

The size of the pFe pool that is available for conversion to the dissolved phase on the time scale of particle residence time in the ocean depends on the process by which the Fe is mobilized. The fastest mobilization processes are probably, in decreasing order, regeneration of biogenic Fe, desorption of surface-complexed Fe, and dissolution of iron-containing biogenic Si. The dissolution of Fe oxyhydroxides and Fecontaining aluminosilicates are probably one or more orders of magnitude slower. The ligand-based leach 18 is thought to access adsorbed Fe as well as some portion of poorly crystalline Fe oxyhydroxides.<sup>63</sup> The pool of pFe that is available for desorption is likely significantly smaller than this measured pool. Indeed, synchrotron X-ray absorption spectroscopy showed that much of the water column pFe formed at shelf depths was in the form of Fe oxyhydroxides,<sup>21</sup> which are unlikely to be a source of Fe through any of the fast mobilization processes. However, we can estimate the size of the organic matter and biogenic Si-associated pools of Fe associated with suspended particles. Assuming an upper limit Fe/P ratio of 5 mmol/mol in organic matter<sup>64</sup> and suspended particulate P concentrations of ~2 nmol/L found between 600 and 2000 m,<sup>22</sup> the pool of biogenic Fe available for

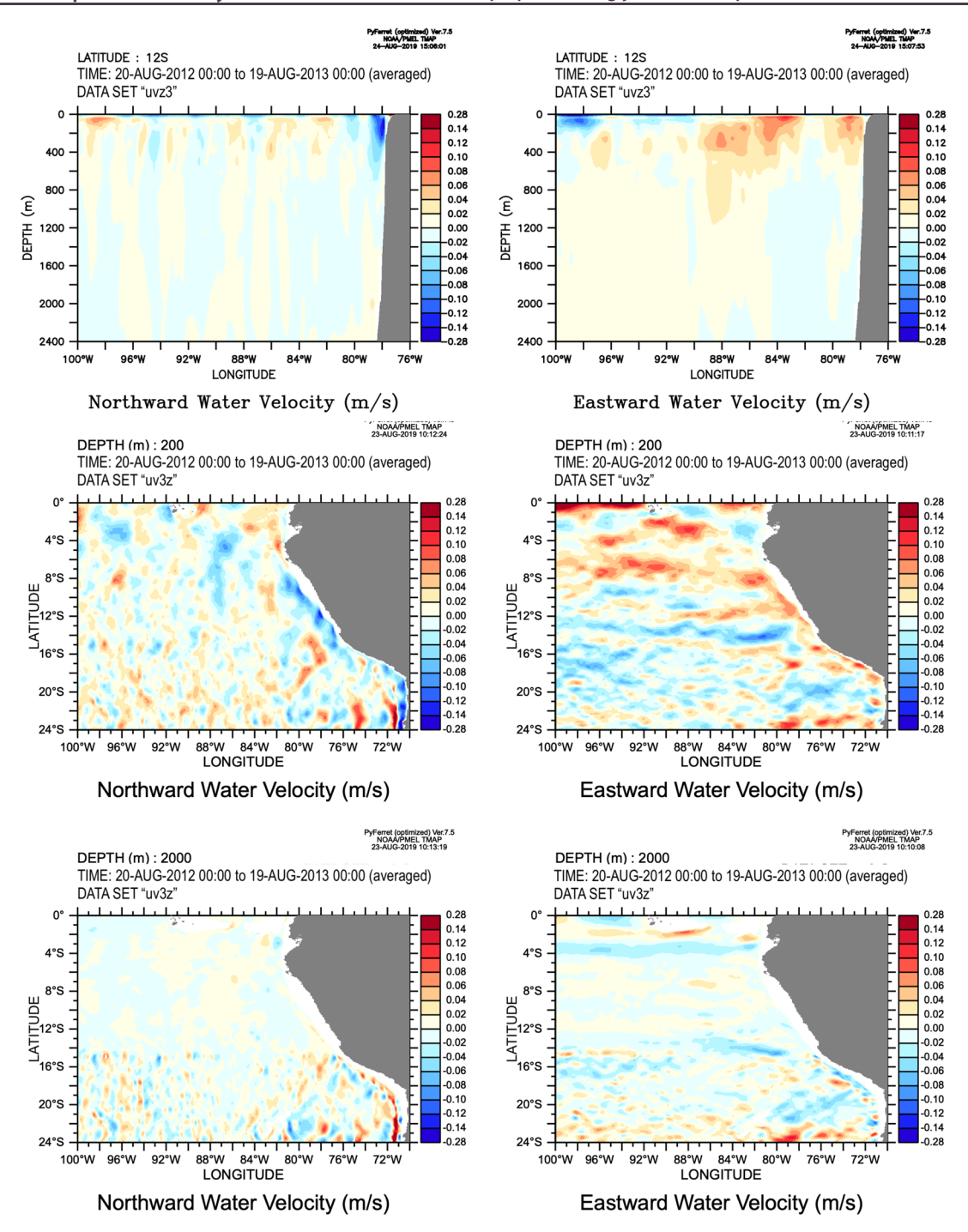


Figure 7. Northward (v) (left column) and Eastward (u) (right column) water velocities from the HYCOM + NCODA Global 1/12° Analysis model. Depth sections along 12°S (top row), isosurface maps at 200 m (middle row), and 2000 m (bottom row). Native hycom data are interpolated to a uniform 0.08° lat/long grid to 40 standard z-levels. Data extracted from GLBu0.08, expt 90.9 and averaged over the year (Aug 20, 2012–Aug 19, 2013) preceding the GP16 occupation.

regeneration is ~10 pmol/L, which is at the lower limit of what is required. Assuming an upper limit Fe/Si ratio of 1.3 mmol/mol<sup>58</sup> and biogenic Si concentrations of 45–120 nM between 600 and 2000 m,<sup>59</sup> the pool of Si-associated Fe available for release from the dissolution of biogenic Si is 60–155 pmol/L. Biogenic Si-associated Fe in suspended particles may thus provide an adequate pool of labile particulate iron to potentially supply slope depths with dFe if the majority of the biogenic Si pool were to dissolve and release its associated Fe into solution, but the isotopic composition of this pool is

unknown. Overall, the potential input of dFe from sinking and suspended particles cannot be ruled out as a contributor to the slope dFe plume.

**Differences in Sink Strength.** We have so far focused on the supply of dissolved Fe in the shallow and midslope plumes, but loss mechanisms are equally important to consider. Loss of particle reactive TEIs due to scavenging is usually described as a function of the concentration of the TEI in the dissolved phase and the particle concentration.<sup>2,65</sup> Higher particle

concentrations provide more surface binding sites for TEIs to sorb to, thereby increasing sorption rates.

Particle concentrations usually decrease quickly with depth, so scavenging rates are generally expected to decrease with depth on the basis of this alone. However, resuspension of sediments can lead to suspended particle concentrations in nepheloid layers approaching those of near surface concentrations. 66 There was only one near-bottom suspended particle mass measurement made below 500 m on the Peru continental slope, and this showed a relatively prominent nepheloid layer at 2000 m that elevates those near-bottom concentrations to be comparable to particle concentrations at  $\sim 200$  m ( $\sim 25 \mu g/$ L) (Figure 6E). Although particle concentrations are similar, the benthic flux and thus near-bottom concentrations of dFe are higher at shelf depths than at slope depths, which should increase scavenging rates at shelf depths. For Fe, however, the redox state, organic complexation, and physicochemical speciation of the dissolved phase is at least as important as its concentration for determining scavenging rates, <sup>67</sup> since in addition to sorption Fe is extremely insoluble in its Fe(III) oxidation state and is easily lost by precipitation into the solid phase unless otherwise stabilized.

As discussed above, dFe is primarily in the Fe(II) form at shelf depths and in the Fe(III) form at slope depths. The usual oxidants for Fe(II) in the ocean,  $O_2$  and  $H_2O_2$ , are extremely low<sup>44,68</sup> in the ODZ at shelf depths, but Fe(II) oxidation rates could still be estimated from modeling water column Fe(II) profiles, suggesting that another oxidant is at work.<sup>44</sup> Previous investigators proposed that nitrite or nitrate were oxidizing Fe(II) in the Peruvian ODZ in the absence of  $O_2$ .<sup>21,69</sup>

It is instructive to compare the fate of dFe(II) that is oxidized at shelf depths compared to slope depths. As we argue above, the reductive dissolution of Fe in sediments is likely supplying Fe for both the shelf and slope dFe plumes. At shelf depths, dFe(II) can freely diffuse into the overlying oxygen deficient water column because oxidation rates are slow, but the dFe(II) appears to be eventually oxidized by nitrite or nitrate in the water column. Interestingly, the water column oxidation of dFe(II) appears to generate filterable pFe(III) (Figure 2), whereas the at least partial oxidation of dFe(II) in the upper few oxygenated centimeters of slope sediments appears to lead to a form of dFe(III) that is resistant to precipitation.

It is unclear why the water column versus the porewater oxidation of dFe(II) should result in stable dFe(III) in the latter case but not the former. The most obvious difference between the two environments is that the water column environment can be orders of magnitude more dilute in many inorganic and organic species than the porewater environment. Porewater DOC concentrations in the upper 6 cm of a box core taken around 1500 m a few hundred kilometers south of our sampling stations were 0.9–1.7 mmol C/L, 70 compared to <0.08 mmol C/L in the upper 100 m of the water column. The DOC-rich porewater environment may allow soluble and colloidal organic ligands to compete with the precipitation of Fe oxyhydroxides, thus keeping oxidized Fe in the dissolved ( $<0.2 \mu m$ ) phase. The decreasing concentrations of LFe with distance at both shelf and slope depths (Figure 3) support a potential porewater source of ligands. In contrast, the more dilute DOC and thus ligand concentrations of even upper water column waters result in ligand complexation rates that are too slow to compete with authigenic and/or microbially mediated precipitation and aggregation of Fe oxyhydroxides

into filterable and sinking particles, which are quickly lost from the water column.

**Differences in Circulation.** Differences in the circulation at shelf and slope depths are also important factors affecting the delivery of margin dFe into the interior. The central Peru Current System is a turbulent regime characterized by significant eddy activity with both models<sup>72</sup> and observations<sup>73–75</sup> showing abundant mesoscale eddies. Cold core rings from the Gulf Stream have been argued to be a significant cross-shelf transport mechanism of iron to the subtropical North Atlantic.<sup>76</sup> While the dynamics of a western versus eastern boundary current is quite different, mesoscale eddies have also been suggested as mechanisms for cross shelf transport in the Peru upwelling system.<sup>44</sup>

Eddies and filaments should cause diffusion-like transport of iron into the interior at all depths. Using the distribution of  $^{228}$ Ra, a radioisotope produced from the decay of  $^{232}$ Th in sediments with a half-life of 5.75 years, horizontal diffusivities of  $K_{\rm H,shelf} = 663$  m<sup>2</sup>/s and  $K_{\rm H,slope} = 46$  m<sup>2</sup>/s were estimated. Since the diffusive flux is the product of the diffusivity and the gradient in concentration, we would expect higher offshore diffusive transport at shelf depths than at slopes depths because of both their higher diffusivities and steeper Fe gradients.

To estimate advective velocities, we examined output from HYCOM, a high-resolution (1/12°) eddy-resolving, data-assimilative ocean circulation model (http://hycom.org). Model output shows highly variable flow from day to day along the Peru margin, as expected for a region with mesoscale variability. When averaged over the time of our occupation (not shown) or over a year preceding our occupation, prevailing water velocities are eastward (toward the margin) and southward in the upper 400 m at 12°S and along the Peru margin from 6 to 18°S (Figure 7), largely reflecting the eastward component of the poleward Peru–Chile Undercurrent (PCU). Mean horizontal flow is weaker below about 800 m at 12°S but is generally westward and northward along a large portion of the Chile–Peru margin at 2000 m (Figure 7).

We can make two conclusions based on this cursory examination of transport terms at shelf and slope depths: (1) the much weaker circulation at slope depths is unlikely to cause the sediment resuspension observed at 2000 m, and (2) the advective regime is more conducive to transporting benthic Fe flux into the interior from slope rather than from shelf depths. At shelf depths, the stronger horizontal diffusive flux toward the interior may potentially counteract and overcome the advective flux toward the margin. In comparison, at slope depths both advection and diffusion should transport Fe toward the interior.

**Sediment Redistribution.** Mechanisms that promote sediment redistribution can enhance dFe sources to the water column by enhancing benthic flux of dFe from sediment porewaters and by resuspending sediment particles into the water column, where they can supply Fe to the aqueous phase by dissolution, desorption, or remineralization, as discussed in the Fe sources section above.

Downslope Sediment Transport. The depths at which the strong poleward flowing undercurrent runs along the sea floor (cf. Figure 7) is reflected in seabed morphological features, including mudwaves between 250 and 400 m water depth. Sediment accumulation can only occur in the shadow of the undercurrent, and indeed there is an organic carbon-rich mud lens close to the shelf break off Callao at 180 m, 77

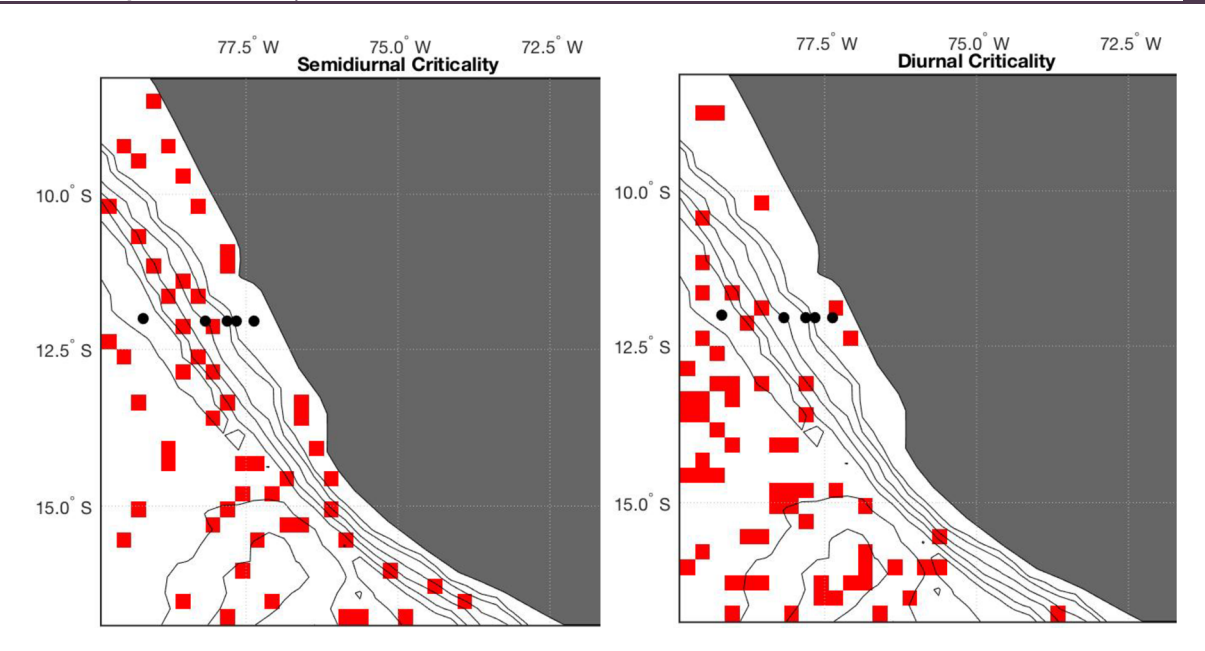


Figure 8. An examination of criticality of semidiurnal (left) or diurnal (right) internal tides in the region surrounding the GP16 transect (stations 1-5 marked as filled black circles; contour lines are the 500, 1000, 2000, 3000, 4000, and 5000 m isobaths). The GMRT bathymetry data set <sup>91</sup> was interpolated to a  $1/4^{\circ}$  grid to match the  $1/4^{\circ}$  WOA13<sup>90</sup> data used to calculate the buoyancy frequency. Grid cells within 20% of criticality are highlighted in red.

approximately between our Stations 2 and 3, which would provide conditions favorable for benthic iron reduction.

The horizontal velocities (Figure 7) suggest that direct resuspension of sediments from the mean circulation is more likely at shelf depths, and yet GP16 observations show greater evidence for sediment resuspension at slope depths below 500 m with elevated near bottom pAl at 750 and 2000 m (Figure 2). The lack of observed sediment resuspension at the shelf break could simply be explained by variability in sediment resuspension events, and that we happened to sample at a quiescent time at the shelf depth. Sediment resuspension events from around the shelf break have been observed: in a survey of the distribution of suspended particulate matter using optical instruments, several intermediate nepheloid layers were observed emanating from the Peru margin at around 200 m at 9°S and 23°S and at 400 m at near 4°S, some of which persisted for several hundred kilometers offshore.<sup>78</sup> The authors suggested advective or diffusive offshore transport.

The observed nepheloid layers at slope depths could be triggered by sediment mobilization at shallower depths, which are then transported downslope by gravitational processes. The locations of highest sediment resuspension at 750 and 2000 m are also where there is a break in the angle of the slope (Figure 1), which may act as depocenters of sediment originating upslope that may be easily resuspended. This downslope sediment transport could also induce turbulence which would act to increase the benthic flux of Fe out of sediment porewaters.

Indeed, there is geochemical evidence for sediment redistribution from the shelf and upper slope. Both geomorphic and <sup>210</sup>Pb evidence indicate that regular sediment slumping occurs on the time scale of decades on the Peru margin, <sup>14,47,79</sup> transporting sediments downslope and laterally across the margin. Further, this region is located in an area of high seismicity with high magnitude (>6 in Richter scale) earthquakes occurring every few years. In fact, a magnitude 7.1 earthquake occurred approximately 500 km southeast of our

cruise track (15.89°S, 74.511°W) on September 25, 2013, just one month prior to the start of the GP16 cruise. Although only weak shaking was reported around 12°S, 80 this is a clear mechanism to destabilize sediment on the continental margin.

Numerous cross-shelf and cross-slope channels in this area of the Peru margin observed from detailed echo-sounder profiles are interpreted as conduits for downslope sediment transport but are currently partly filled with sediment and thought to be inactive.<sup>77</sup>

Internal Waves. An alternative mechanism to resuspend particles at the margin is through the action of internal waves. If the angle of internal wave travel is similar to the angle of the continental slope, it is said to be critical.

The angle of internal wave travel, c, is calculated as

$$c = \left(\frac{\sigma^2 - f^2}{N^2 - \sigma^2}\right)$$

where  $\sigma$  is the internal wave frequency, f is the inertial frequency (Coriolis parameter), and  $N \equiv \sqrt{-\frac{g}{\rho} \frac{\mathrm{d}\rho}{\mathrm{d}z}}$  is the buoyancy (Brunt-Väisälä) frequency, where  $\rho$  is the potential density, and g is the gravitational acceleration. Criticality elevates turbulence dissipation and mixing, which may lead to sediment resuspension and the formation of bottom or intermediate nepheloid layers that can spread into the ocean interior. Criticality should result in the highest bottom velocities and shear stresses. Internal waves whose angle of travel is greater than the angle of the slope are "transmissive" and may result in bottom velocities that increase upslope. Finally, internal wave angles that are less than the slope are "reflective" and do not transfer much energy to the slope.

The influence of the dominant  $M_2$  (semidiurnal) tide on sediment resuspension in the upper 1200 m of the continental slope was investigated in a series of transects from 8°S to 12°S using multibeam bathymetric data. These investigators found that near-critical slopes frequently occur between 500

and 1000 m. Low sediment and mass accumulation rates and phosphorite hard grounds, an erosion indicator, were found at near-critical water depths, 88,89 suggesting that near-critical and transmissive internal waves resuspend and carry sediments upslope where the Peru Coastal Undercurrent may transport them away.<sup>89</sup> A diurnal tide or near-initial gravity wave could provide the energy to resuspend sediments at 2000 m on the GP16 transect.<sup>59</sup> We extended the analysis to examine criticality in the region surrounding the GP16 transect using annual climatologies (2005-2012) of T, S data from the World Ocean Atlas 2013 at 1/4° resolution 90 to calculate the buoyancy frequency using the Thermodynamic Equation of Seawater toolbox (TEOS-10; McDougall and Barker, 2011) and the Global Multi Resolution Topography data set<sup>91</sup> interpolated to the WOA2013 grid to calculate the slope and assuming a semidiurnal or diurnal tide frequency. Ignoring the abyssal depths, we confirm that semidiurnal waves are more likely to be near critical on the continental margin than diurnal waves, although there are a few locations in which diurnal waves are near critical (Figure 8). Although not all points along the margin are near-critical with respect to semidiurnal or diurnal waves, the prevalence of criticality is high enough that internal waves are a plausible mechanism to be important generally for sediment resuspension along continental margins.

Both pAl and <sup>228</sup>Ra are elevated at ~2000 m and decrease in concentration smoothly away from the margin (Figure 2). Even though elevated pAl persists to 89°W, elevated <sup>228</sup>Ra disappears before 84°W because it is decaying as it is diffusing into the interior (Figure 2). <sup>25</sup> It takes three e-folding times (~25 years for  $1/\lambda = 8.3$  yrs) for <sup>228</sup>Ra to decay away to 5% of its original value. This gives us a minimum estimate for the time it takes to transport pAl to 84°W. The smooth decrease in <sup>228</sup>Ra activities <sup>25</sup> and in pAl concentrations (Figure 2) with distance from the coast suggests a constant source from the margin and consequently demands a relatively consistent way to enhance benthic flux and resuspension. An internal wave mechanism satisfies this requirement for a consistent source. Gravitational processes that lead to downslope sediment transport processes could potentially also satisfy this requirement if they are frequent enough.

# **■** IMPLICATIONS FOR OTHER MARGINS

It was recently suggested that margins overlaid by OMZ waters might be particularly effective at generating deep plumes of dFe because of the high fluxes of Fe oxyhydroxides generated in the OMZ to slope sediments. 11 Indeed, to maintain a solid phase Fe/Al ratio that is approximately crustal, as observed in near-bottom waters at Station 5, there must be a steady state supply of easily dissolvable iron either from the water column above or from upslope sediments that balances a loss of Fe from the solid phase due to reductive and nonreductive dissolution. Besides the Peru margin feature discussed here, it was noted11 that elevated dFe was observed from the continental slope in the western Indian Ocean, 92 off the Namibian coast, 93 and off Senegal. 94 There is also elevated dFe from slope depths in several transects intersecting the Aleutian and Kuril-Kamchatka margins. 95 It is clear that many continental slopes are an important source of dFe into the interior, but the mechanisms responsible for their release of dFe require further study and likely vary from margin to

Not only are careful studies of benthic fluxes of TEIs quite limited, 3,7 but there are even fewer that have directly studied

slope depths. As the basin section portion of the international GEOTRACES Programme winds down, attention should turn to process studies that focus on how variations in sediment and overlying water column characteristics affect TEI exchange.

## CONCLUSIONS

The margin end of the U.S. GEOTRACES GP16 transect in the Eastern Tropical South Pacific off the coast of Peru revealed several surprises in the role of continental margins as a source of iron to the ocean interior. As expected, near-bottom dissolved Fe was highest at shelf depths where dissolved oxygen concentrations were lowest and generally decreased with depth as oxygen concentrations increased out of the OMZ. However, contrary to expectations the lateral penetration of benthic dissolved Fe was much greater from midslope depths (1000–3000 m), where oxygen concentrations exceeded 100  $\mu$ M, than at shelf and upper slope depths (50–200 m), where oxygen concentrations were below detection.

The most effective margin sources of dFe to the water column will be those in which the dFe flux from porewaters to overlying waters is high, and the effluxed dFe is stabilized in a form that is resistant to scavenging. Scores of previous studies have shown that margins with high organic matter oxidation and low bottom water oxygen concentrations result in the highest benthic Fe flux, but Peru OMZ studies show that this iron appears to be less persistent than expected. As long as the effluxed dFe remains in Fe(II) form, it is quite stable, but the water column oxidation of this dFe(II) by any oxidant (e.g., O2, H2O2, NO3-, NO2-) appears to generate filterable (and sinkable) pFe. In contrast, the oxidation of porewater dFe(II) in the upper centimeters of sediments where oxygen penetrates appears to generate stabilized dFe(III) that can remain in solution and is resistant to scavenging. Figure 9 summarizes these ideas. At shelf depths, the main source of iron is from

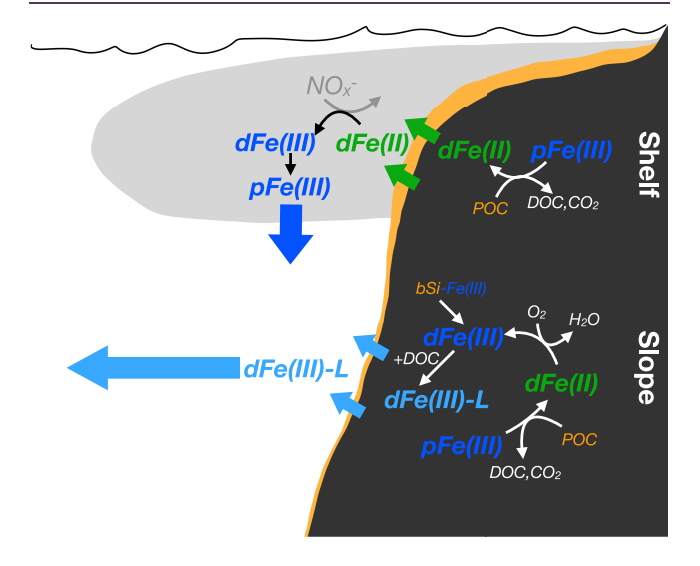


Figure 9. Schematic of the main sources and sinks of dFe at shelf and slope depths at the Peru margin. Block arrows represent diffusive and advective transport processes. Thin arrows represent oxidation, reduction, complexation, and precipitation reactions. Oxygen deficient waters at shelf depths are shaded light gray. Biogenic sediments are shaded light orange. POC: particulate organic carbon. DOC: dissolved organic carbon. dFe(III)-L: ligand-bound dFe(III). bSi-Fe(III): biogenic silica with adsorbed or structural Fe(III).

reductive dissolution of pFe(III) in shelf sediments fueled by organic carbon remineralization from biogenic sediments (orange layer). The dFE(II) diffuses into oxygen deficient (light gray shading) overlying waters but is oxidized close to shore, likely by nitrate or nitrite, and precipitates to pFe(III), which sinks. At slope depths, moderate POC supply to the sediments can still fuel reductive dissolution in the sediments a few centimeters below the sediment—water interface. Upward diffusing dFe(II) is oxidized to dFe(III) in the oxygenated porewaters toward the sediment—water interface but high DOC concentrations in porewaters supply Fe-binding ligands that complex dFe(III), keeping it in solution. Ligand-bound dFe(III) is thus stabilized from removal and can be advected into the interior.

We postulate that margin sediments that receive a moderate amount of organic carbon flux, characterized by oxygenated bottom waters but shallow oxygen penetration into the sediments, may be the most efficient sources of persistent dFe into the water column. Although the magnitude of the benthic Fe flux from these types of margins may be less than that from highly productive margins overlain by oxygen deficient waters, it appears that the iron that does emanate from these margins is particularly persistent. We speculate that iron from these margins is stabilized by soluble and/or colloidal organic ligands generated in the DOC-rich porewater environment, and that dFe in this form is particularly resistant to scavenging. Process studies that focus on sediment processes in these environments are needed to test these ideas.

#### METHODS

When available, data were taken from the GEOTRACES Intermediate Data Product 2017 version 2 (IDP2017 v2).<sup>26</sup> The specific IDP2017 parameters used were Fe D CONC -BOTTLE for dissolved Fe,9 Fe 56 54 D DELTA BOT-TLE<sup>10</sup> Fe 56 54 SPL DELTA PUMP<sup>18</sup> for the isotopic compositions of dFe and leachable pFe, the sum of the strong Fe ligand concentrations (L1Fe\_D\_CONC\_BOTTLE +L2Fe D CONC BOTTLE) for L<sub>Fe</sub>, where L<sub>1</sub>Fe is for log  $K_{\text{FeL,Fe'}}^{\text{cond}} > 12$  and  $L_2$ Fe is for log  $K_{\text{FeL,Fe'}}^{\text{cond}} = 11-12$  binding classes, 20 Fe\_TP\_CONC\_BOTTLE and Al\_TP\_CONC\_-BOTTLE for pFe and pAl from bottle filtration, respectively, <sup>23,96</sup> Fe\_SPT\_CONC\_PUMP for small pFe from in situ pump filtration, <sup>21,22</sup> and Ra\_228\_D\_CONC\_PUMP for <sup>228</sup>Ra. <sup>25</sup> When multiple data sets were submitted (e.g., for dFe), the value in the IDP2017 represents the median of all data sets.<sup>26</sup> All parameters reported here with suffix "CONC BOTTLE" were sampled from Teflon coated GOflo bottles on the GEOTRACES carousel filtered through a 0.2 μm Acropak Supor200 capsule filter 97,98 for dissolved components or onto a 0.45  $\mu m$  Supor membrane filter for particles. All parameters with suffix "CONC PUMP" were sampled using McLane in situ pumps.<sup>59</sup> Particulate components with the suffix "SPT" and "SPL" are the Small Particulate (0.8  $\mu$ m-51  $\mu$ m) Total digest or Small Particulate Leachable fraction of in situ pump samples. This fraction represents approximately 80% of the total size distribution of these parameters.<sup>22</sup> Note that Figure 2 shows pFe and pAl from bottle filtration because of their higher spatial resolution than in situ pump particles, whereas Figure 5 shows pFe and pAl from in situ pump filtration, since these are the samples that were examined by synchrotron X-ray methods. N-star was calculated using the macro in Ocean Data View:  $^{99}$  N-star = 0.87 \* (Nitrate -16\*Phosphate +0.29) $^{100}$ 

Si-star was calculated as Si-star = Silicate - Nitrate  $^{101}$ 

# AUTHOR INFORMATION

#### **Corresponding Author**

Phoebe J. Lam — Department of Ocean Sciences, University of California, Santa Cruz, Santa Cruz, California, United States; orcid.org/0000-0001-6609-698X; Email: pjlam@ucsc.edu

#### **Authors**

Maija I. Heller – Escuela de Ciencias del Mar, Facultad de Ciencias del Mar y Geografiá, Pontifica Universidad Católica de Valparaiso, 2950, Chile; Instituto Milenio de Oceanografia, Concepción, Chile

Paul E. Lerner – NASA Goddard Institute for Space Studies, New York City, New York 10025, United States

James W. Moffett – Departments of Biological Sciences and Earth Sciences, University of Southern California, Los Angeles, California 90089, United States

**Kristen N. Buck** – College of Marine Science, University of South Florida, St. Petersburg, Florida 33701, United States

Complete contact information is available at: https://pubs.acs.org/10.1021/acsearthspacechem.0c00066

#### **Notes**

The authors declare no competing financial interest.

#### ACKNOWLEDGMENTS

This work was supported in part by NSF-OCE-1518110, OCE-1441969, NSF OCE-1260279 and NSF OCE-1556400. Many thanks to the GEOTRACES program for supporting synthesis workshops that led to this work, colleagues at UCSC (Carl Lamborg, Chris Edwards, Jerome Fiechter) for stimulating discussions, and the helpful comments from four anonymous reviewers.

#### REFERENCES

- (1) Moore, J. K.; Doney, S. C.; Glover, D. M.; Fung, I. Y. Iron cycling and nutrient-limitation patterns in surface waters of the World Ocean. *Deep Sea Res., Part II* **2001**, 49 (1–3), 463–507.
- (2) Tagliabue, A.; Aumont, O.; DeAth, R.; Dunne, J. P.; Dutkiewicz, S.; Galbraith, E.; Misumi, K.; Moore, J. K.; Ridgwell, A.; Sherman, E.; Stock, C.; Vichi, M.; Völker, C.; Yool, A. How well do global ocean biogeochemistry models simulate dissolved iron distributions? *Global Biogeochemical Cycles* **2016**, *30* (2), 149–174.
- (3) Charette, M. A.; Lam, P. J.; Lohan, M. C.; Kwon, E. Y.; Hatje, V.; Jeandel, C.; Shiller, A. M.; Cutter, G. A.; Thomas, A.; Boyd, P. W.; Homoky, W. B.; Milne, A.; Thomas, H.; Andersson, P. S.; Porcelli, D.; Tanaka, T.; Geibert, W.; Dehairs, F.; Garcia-Orellana, J. Coastal ocean and shelf-sea biogeochemical cycling of trace elements and isotopes: lessons learned from GEOTRACES. *Philos. Trans. R. Soc., A* **2016**, 374, 20160076.
- (4) Anderson, R. F.; Cheng, H.; Edwards, R. L.; Fleisher, M. Q.; Hayes, C. T.; Huang, K. F.; Kadko, D.; Lam, P. J.; Landing, W. M.; Lao, Y.; Lu, Y.; Measures, C. I.; Moran, S. B.; Morton, P. L.; Ohnemus, D. C.; Robinson, L. F.; Shelley, R. U. How well can we quantify dust deposition to the ocean? *Philos. Trans. R. Soc., A* **2016**, 374, 20150285.
- (5) Baker, A. R.; Landing, W. M.; Bucciarelli, E.; Cheize, M.; Fietz, S.; Hayes, C. T.; Kadko, D.; Morton, P. L.; Rogan, N.; Sarthou, G.; Shelley, R. U.; Shi, Z.; Shiller, A.; van Hulten, M. M. P. Trace element and isotope deposition across the air—sea interface: progress and research needs. *Philos. Trans. R. Soc., A* **2016**, 374, 20160190.
- (6) German, C. R.; Casciotti, K. A.; Dutay, J.-C.; Heimbürger, L. E.; Jenkins, W. J.; Measures, C. I.; Mills, R. A.; Obata, H.; Schlitzer, R.; Tagliabue, A.; Turner, D. R.; Whitby, H. Hydrothermal impacts on

- trace element and isotope ocean biogeochemistry. *Philos. Trans. R. Soc., A* 2016, 374, 20160035.
- (7) Homoky, W. B.; Weber, T.; Berelson, W. M.; Conway, T. M.; Henderson, G. M.; van Hulten, M.; Jeandel, C.; Severmann, S.; Tagliabue, A. Quantifying trace element and isotope fluxes at the ocean–sediment boundary: a review. *Philos. Trans. R. Soc., A* **2016**, 374, 20160246.
- (8) Moffett, J. W.; German, C. R. The U.S.GEOTRACES Eastern Tropical Pacific Transect (GP16). *Mar. Chem.* **2018**, 201, 1–5.
- (9) Resing, J. A.; Sedwick, P. N.; German, C. R.; Jenkins, W. J.; Moffett, J. W.; Sohst, B. M.; Tagliabue, A. Basin-scale transport of hydrothermal dissolved metals across the South Pacific Ocean. *Nature* **2015**, 523 (7559), 200–203.
- (10) John, S. G.; Helgoe, J.; Townsend, E.; Weber, T.; DeVries, T.; Tagliabue, A.; Moore, K.; Lam, P.; Marsay, C. M.; Till, C. Biogeochemical cycling of Fe and Fe stable isotopes in the Eastern Tropical South Pacific. *Mar. Chem.* **2018**, *201*, 66–76.
- (11) Moffett, J. W.; German, C. R. Distribution of iron in the Western Indian Ocean and the Eastern tropical South pacific: An inter-basin comparison. *Chem. Geol.* **2020**, 532, 119334.
- (12) Pennington, J. T.; Mahoney, K. L.; Kuwahara, V. S.; Kolber, D. D.; Calienes, R.; Chavez, F. P. Primary production in the eastern tropical Pacific: A review. *Prog. Oceanogr.* **2006**, *69* (2–4), 285–317.
- (13) Strub, P. T.; Mesias, J. M.; Montecino, V.; Ruttlant, J.; Salinas, S., Coastal ocean circulation off Western South America. *In The Global Coastal Ocean. Regional Studies and Syntheses*; Robinson, A. R., Brink, K. H., Eds.; Wiley: New York, 1998; pp 273–314.
- (14) Muñoz, P.; Lange, C. B.; Gutiérrez, D.; Hebbeln, D.; Salamanca, M. A.; Dezileau, L.; Reyss, J. L.; Benninger, L. K. Recent sedimentation and mass accumulation rates based on 210Pb along the Peru–Chile continental margin. *Deep Sea Res., Part II* **2004**, *51* (20), 2523–2541.
- (15) Chavez, F. P.; Messié, M. A comparison of Eastern Boundary Upwelling Ecosystems. *Prog. Oceanogr.* **2009**, 83 (1), 80–96.
- (16) Berelson, W. M.; Haskell, I. W. Z.; Prokopenko, M.; Knapp, A. N.; Hammond, D. E.; Rollins, N.; Capone, D. G. Biogenic particle flux and benthic remineralization in the Eastern Tropical South Pacific. *Deep Sea Res., Part I* **2015**, *99* (0), 23–34.
- (17) Bruland, K. W.; Rue, E. L.; Smith, G. J.; DiTullio, G. R. Iron, macronutrients and diatom blooms in the Peru upwelling regime: brown and blue waters of Peru. *Mar. Chem.* **2005**, 93 (2–4), 81–103.
- (18) Marsay, C. M.; Lam, P. J.; Heller, M. I.; Lee, J.-M.; John, S. G. Distribution and isotopic signature of ligand-leachable particulate iron along the GEOTRACES GP16 East Pacific Zonal Transect. *Mar. Chem.* **2018**, 201, 198–211.
- (19) Cutter, G. A.; Moffett, J. G.; Nielsdóttir, M. C.; Sanial, V. Multiple oxidation state trace elements in suboxic waters off Peru: In situ redox processes and advective/diffusive horizontal transport. *Mar. Chem.* **2018**, 201, 77–89.
- (20) Buck, K. N.; Sedwick, P. N.; Sohst, B.; Carlson, C. A. Organic complexation of iron in the eastern tropical South Pacific: Results from US GEOTRACES Eastern Pacific Zonal Transect (GEOTRACES cruise GP16). *Mar. Chem.* **2018**, 201, 229–241.
- (21) Heller, M. I.; Lam, P. J.; Moffett, J. W.; Till, C. P.; Lee, J.-M.; Toner, B. M.; Marcus, M. A. Accumulation of Fe oxyhydroxides in the Peruvian oxygen deficient zone implies non-oxygen dependent Fe oxidation. *Geochim. Cosmochim. Acta* **2017**, *211*, 174–193.
- (22) Lee, J.-M.; Heller, M. I.; Lam, P. J. Size distribution of particulate trace elements in the U.S. GEOTRACES Eastern Pacific Zonal Transect (GP16). *Mar. Chem.* **2018**, 201, 108–123.
- (23) Ohnemus, D. C.; Torrie, R.; Twining, B. S. Exposing the Distributions and Elemental Associations of Scavenged Particulate Phases in the Ocean Using Basin-Scale Multi-Element Data Sets. *Global Biogeochem. Cycles* **2019**, 33 (6), 725–748.
- (24) Ohnemus, D. C.; Rauschenberg, S.; Cutter, G. A.; Fitzsimmons, J. N.; Sherrell, R. M.; Twining, B. S., Elevated trace metal content of prokaryotic communities associated with marine oxygen deficient zones. *Limnol. Oceanogr.* 2017, 62, 3.

- (25) Sanial, V.; Kipp, L. E.; Henderson, P. B.; van Beek, P.; Reyss, J. L.; Hammond, D. E.; Hawco, N. J.; Saito, M. A.; Resing, J. A.; Sedwick, P.; Moore, W. S.; Charette, M. A. Radium-228 as a tracer of dissolved trace element inputs from the Peruvian continental margin. *Mar. Chem.* **2018**, 201, 20–34.
- (26) Schlitzer, R.; Anderson, R. F.; Dodas, E. M.; Lohan, M.; Geibert, W.; Tagliabue, A.; Bowie, A.; Jeandel, C.; Maldonado, M. T.; Landing, W. M.; Cockwell, D.; Abadie, C.; Abouchami, W.; Achterberg, E. P.; Agather, A.; Aguliar-Islas, A.; van Aken, H. M.; Andersen, M.; Archer, C.; Auro, M.; de Baar, H. J.; Baars, O.; Baker, A. R.; Bakker, K.; Basak, C.; Baskaran, M.; Bates, N. R.; Bauch, D.; van Beek, P.; Behrens, M. K.; Black, E.; Bluhm, K.; Bopp, L.; Bouman, H.; Bowman, K.; Bown, J.; Boyd, P.; Boye, M.; Boyle, E. A.; Branellec, P.; Bridgestock, L.; Brissebrat, G.; Browning, T.; Bruland, K. W.; Brumsack, H.-J.; Brzezinski, M.; Buck, C. S.; Buck, K. N.; Buesseler, K.; Bull, A.; Butler, E.; Cai, P.; Mor, P. C.; Cardinal, D.; Carlson, C.; Carrasco, G.; Casacuberta, N.; Casciotti, K. L.; Castrillejo, M.; Chamizo, E.; Chance, R.; Charette, M. A.; Chaves, J. E.; Cheng, H.; Chever, F.; Christl, M.; Church, T. M.; Closset, I.; Colman, A.; Conway, T. M.; Cossa, D.; Croot, P.; Cullen, J. T.; Cutter, G. A.; Daniels, C.; Dehairs, F.; Deng, F.; Dieu, H. T.; Duggan, B.; Dulaquais, G.; Dumousseaud, C.; Echegoyen-Sanz, Y.; Edwards, R. L.; Ellwood, M.; Fahrbach, E.; Fitzsimmons, J. N.; Russell Flegal, A.; Fleisher, M. Q.; van de Flierdt, T.; Frank, M.; Friedrich, J.; Fripiat, F.; Fröllje, H.; Galer, S. J. G.; Gamo, T.; Ganeshram, R. S.; Garcia-Orellana, J.; Garcia-Solsona, E.; Gault-Ringold, M.; George, E.; Gerringa, L. J. A.; Gilbert, M.; Godoy, J. M.; Goldstein, S. L.; Gonzalez, S. R.; Grissom, K.; Hammerschmidt, C.; Hartman, A.; Hassler, C. S.; Hathorne, E. C.; Hatta, M.; Hawco, N.; Hayes, C. T.; Heimbürger, L.-E.; Helgoe, J.; Heller, M.; Henderson, G. M.; Henderson, P. B.; van Heuven, S.; Ho, P.; Horner, T. J.; Hsieh, Y.-T.; Huang, K.-F.; Humphreys, M. P.; Isshiki, K.; Jacquot, J. E.; Janssen, D. J.; Jenkins, W. J.; John, S.; Jones, E. M.; Jones, J. L.; Kadko, D. C.; Kayser, R.; Kenna, T. C.; Khondoker, R.; Kim, T.; Kipp, L.; Klar, J. K.; Klunder, M.; Kretschmer, S.; Kumamoto, Y.; Laan, P.; Labatut, M.; Lacan, F.; Lam, P. J.; Lambelet, M.; Lamborg, C. H.; Le Moigne, F. A. C.; Le Roy, E.; Lechtenfeld, O. J.; Lee, J.-M.; Lherminier, P.; Little, S.; López-Lora, M.; Lu, Y.; Masque, P.; Mawji, E.; McClain, C. R.; Measures, C.; Mehic, S.; Barraqueta, J.-L. M.; van der Merwe, P.; Middag, R.; Mieruch, S.; Milne, A.; Minami, T.; Moffett, J. W.; Moncoiffe, G.; Moore, W. S.; Morris, P. J.; Morton, P. L.; Nakaguchi, Y.; Nakayama, N.; Niedermiller, J.; Nishioka, J.; Nishiuchi, A.; Noble, A.; Obata, H.; Ober, S.; Ohnemus, D. C.; van Ooijen, J.; O'Sullivan, J.; Owens, S.; Pahnke, K.; Paul, M.; Pavia, F.; Pena, L. D.; Peters, B.; Planchon, F.; Planquette, H.; Pradoux, C.; Puigcorbé, V.; Quay, P.; Queroue, F.; Radic, A.; Rauschenberg, S.; Rehkämper, M.; Rember, R.; Remenyi, T.; Resing, J. A.; Rickli, J.; Rigaud, S.; Rijkenberg, M. J. A.; Rintoul, S.; Robinson, L. F.; Roca-Martí, M.; Rodellas, V.; Roeske, T.; Rolison, J. M.; Rosenberg, M.; Roshan, S.; Rutgers van der Loeff, M. M.; Ryabenko, E.; Saito, M. A.; Salt, L. A.; Sanial, V.; Sarthou, G.; Schallenberg, C.; Schauer, U.; Scher, H.; Schlosser, C.; Schnetger, B.; Scott, P.; Sedwick, P. N.; Semiletov, I.; Shelley, R.; Sherrell, R. M.; Shiller, A. M.; Sigman, D. M.; Singh, S. K.; Slagter, H. A.; Slater, E.; Smethie, W. M.; Snaith, H.; Sohrin, Y.; Sohst, B.; Sonke, J. E.; Speich, S.; Steinfeldt, R.; Stewart, G.; Stichel, T.; Stirling, C. H.; Stutsman, J.; Swarr, G. J.; Swift, J. H.; Thomas, A.; Thorne, K.; Till, C. P.; Till, R.; Townsend, A. T.; Townsend, E.; Tuerena, R.; Twining, B. S.; Vance, D.; Velazquez, S.; Venchiarutti, C.; Villa-Alfageme, M.; Vivancos, S. M.; Voelker, A. H. L.; Wake, B.; Warner, M. J.; Watson, R.; van Weerlee, E.; Alexandra Weigand, M.; Weinstein, Y.; Weiss, D.; Wisotzki, A.; Woodward, E. M. S.; Wu, J.; Wu, Y.; Wuttig, K.; Wyatt, N.; Xiang, Y.; Xie, R. C.; Xue, Z.; Yoshikawa, H.; Zhang, J.; Zhang, P.; Zhao, Y.; Zheng, L.; Zheng, X.-Y.; Zieringer, M.; Zimmer, L. A.; Ziveri, P.; Zunino, P.; Zurbrick, C. The GEOTRACES Intermediate Data Product 2017. Chem. Geol. 2018, 493, 210-223.
- (27) Peters, B. D.; Jenkins, W. J.; Swift, J. H.; German, C. R.; Moffett, J. W.; Cutter, G. A.; Brzezinski, M. A.; Casciotti, K. L. Water mass analysis of the 2013 US GEOTRACES eastern Pacific zonal transect (GP16). *Mar. Chem.* **2018**, 201, 6–19.

- (28) Johnson, K. S.; Gordon, R. M.; Coale, K. H. What controls dissolved iron concentrations in the world ocean? *Mar. Chem.* **1997**, 57 (3–4), 137–161.
- (29) Roshan, S.; Wu, J. Mid-depth plume of colloidal Fe in the Eastern Tropical South Pacific. Manuscript in preparation.
- (30) Burdige, D. J. The biogeochemistry of manganese and iron reduction in marine sediments. *Earth-Sci. Rev.* **1993**, *35* (3), 249–284.
- (31) Severmann, S.; McManus, J.; Berelson, W. M.; Hammond, D. E. The continental shelf benthic iron flux and its isotope composition. *Geochim. Cosmochim. Acta* **2010**, 74 (14), 3984–4004.
- (32) Elrod, V. A.; Berelson, W. M.; Coale, K. H.; Johnson, K. S. The flux of iron from continental shelf sediments: A missing source for global budgets. *Geophys. Res. Lett.* **2004**, *31* (12), L12307.
- (33) Dale, A. W.; Nickelsen, L.; Scholz, F.; Hensen, C.; Oschlies, A.; Wallmann, K. A revised global estimate of dissolved iron fluxes from marine sediments. *Global Biogeochemical Cycles* **2015**, 29 (5), 691–707
- (34) Noffke, A.; Hensen, C.; Sommer, S.; Scholz, F.; Bohlen, L.; Mosch, T.; Graco, M.; Wallmann, K. Benthic iron and phosphorus fluxes across the Peruvian oxygen minimum zone. *Limnol. Oceanogr.* **2012**, *57* (3), 851–867.
- (35) Scholz, F.; Hensen, C.; Noffke, A.; Rohde, A.; Liebetrau, V.; Wallmann, K. Early diagenesis of redox-sensitive trace metals in the Peru upwelling area response to ENSO-related oxygen fluctuations in the water column. *Geochim. Cosmochim. Acta* **2011**, 75 (22), 7257–7276.
- (36) Morgan, B.; Lahav, O. The effect of pH on the kinetics of spontaneous Fe(II) oxidation by O2 in aqueous solution basic principles and a simple heuristic description. *Chemosphere* **2007**, *68* (11), 2080–2084.
- (37) Taillefert, M.; Beckler, J. S.; Carey, E.; Burns, J. L.; Fennessey, C. M.; DiChristina, T. J. Shewanella putrefaciens produces an Fe(III)-solubilizing organic ligand during anaerobic respiration on insoluble Fe(III) oxides. *J. Inorg. Biochem.* **2007**, *101* (11), 1760–1767.
- (38) Beckler, J. S.; Jones, M. E.; Taillefert, M. The origin, composition, and reactivity of dissolved iron(III) complexes in coastal organic- and iron-rich sediments. *Geochim. Cosmochim. Acta* **2015**, *152* (0), 72–88.
- (39) Beckler, J. S.; Kiriazis, N.; Rabouille, C.; Stewart, F. J.; Taillefert, M. Importance of microbial iron reduction in deep sediments of river-dominated continental-margins. *Mar. Chem.* **2016**, *178*, 22–34.
- (40) Bundy, R. M.; Jiang, M.; Carter, M.; Barbeau, K. A. Iron-Binding Ligands in the Southern California Current System: Mechanistic Studies. *Frontiers in Marine Science* **2016**, *3*, 27.
- (41) Velasquez, I. B.; Ibisanmi, E.; Maas, E. W.; Boyd, P. W.; Nodder, S.; Sander, S. G. Ferrioxamine Siderophores Detected amongst Iron Binding Ligands Produced during the Remineralization of Marine Particles. *Front. Mar. Sci.* **2016**, *3*, 172.
- (42) Bressac, M.; Guieu, C.; Ellwood, M. J.; Tagliabue, A.; Wagener, T.; Laurenceau-Cornec, E. C.; Whitby, H.; Sarthou, G.; Boyd, P. W. Resupply of mesopelagic dissolved iron controlled by particulate iron composition. *Nat. Geosci.* **2019**, *12* (12), 995–1000.
- (43) Klar, J. K.; Homoky, W. B.; Statham, P. J.; Birchill, A. J.; Harris, E. L.; Woodward, E. M. S.; Silburn, B.; Cooper, M. J.; James, R. H.; Connelly, D. P.; Chever, F.; Lichtschlag, A.; Graves, C. Stability of dissolved and soluble Fe(II) in shelf sediment pore waters and release to an oxic water column. *Biogeochemistry* **2017**, *135* (1), 49–67.
- (44) Croot, P. L.; Heller, M. I.; Wuttig, K. Redox Processes Impacting the Flux of Iron(II) from Shelf Sediments to the OMZ along the Peruvian Shelf. ACS Earth and Space Chemistry 2019, 3 (4), 537–549.
- (45) Lenstra, W. K.; Hermans, M.; Séguret, M. J. M.; Witbaard, R.; Behrends, T.; Dijkstra, N.; van Helmond, N. A. G. M.; Kraal, P.; Laan, P.; Rijkenberg, M. J. A.; Severmann, S.; Teacă, A.; Slomp, C. P., The shelf-to-basin iron shuttle in the Black Sea revisited. *Chem. Geol.* **2019**, *511*, 314–341.

- (46) Thamdrup, B.; Canfield, D. E. Pathways of carbon oxidation in continental margin sediments off central Chile. *Limnol. Oceanogr.* **1996**, *41* (8), 1629–1650.
- (47) Levin, L.; Gutiérrez, D.; Rathburn, A.; Neira, C.; Sellanes, J.; Muñoz, P.; Gallardo, V.; Salamanca, M. Benthic processes on the Peru margin: a transect across the oxygen minimum zone during the 1997–98 El Niño. *Prog. Oceanogr.* **2002**, *53* (1), 1–27.
- (48) Millero, F. J.; Sotolongo, S.; Izaguirre, M. The Oxidation-Kinetics of Fe(II) in Seawater. *Geochim. Cosmochim. Acta* **1987**, *51* (4), 793–801.
- (49) Bates, N. R. Seawater Carbonate Chemistry Distributions Across the Eastern South Pacific Ocean Sampled as Part of the GEOTRACES Project and Changes in Marine Carbonate Chemistry Over the Past 20 Years. *Front. Mar. Sci.* **2018**, *5*, 398.
- (50) Homoky, W. B.; Severmann, S.; Mills, R. A.; Statham, P. J.; Fones, G. R. Pore-fluid Fe isotopes reflect the extent of benthic Fe redox recycling: Evidence from continental shelf and deep-sea sediments. *Geology* **2009**, *37* (8), 751–754.
- (51) Jeandel, C.; Oelkers, E. H. The influence of terrigenous particulate material dissolution on ocean chemistry and global element cycles. *Chem. Geol.* **2015**, 395, 50–66.
- (52) Radic, A.; Lacan, F.; Murray, J. W. Iron isotopes in the seawater of the equatorial Pacific Ocean: New constraints for the oceanic iron cycle. *Earth Planet. Sci. Lett.* **2011**, 306 (1–2), 1–10.
- (53) Homoky, W. B.; John, S. G.; Conway, T. M.; Mills, R. A. Distinct iron isotopic signatures and supply from marine sediment dissolution. *Nat. Commun.* **2013**, *4*, 2143.
- (54) Conway, T. M.; John, S. G. Quantification of dissolved iron sources to the North Atlantic Ocean. *Nature* **2014**, *511* (7508), 212–215
- (55) Brantley, S. L.; Liermann, L. J.; Guynn, R. L.; Anbar, A.; Icopini, G. A.; Barling, J. Fe isotopic fractionation during mineral dissolution with and without bacteria. *Geochim. Cosmochim. Acta* **2004**, *68* (15), 3189–3204.
- (56) Napieralski, S. A.; Buss, H. L.; Brantley, S. L.; Lee, S.; Xu, H.; Roden, E. E. Microbial chemolithotrophy mediates oxidative weathering of granitic bedrock. *Proc. Natl. Acad. Sci. U. S. A.* **2019**, 116, 26394.
- (57) Cheize, M.; Planquette, H. F.; Fitzsimmons, J. N.; Pelleter, E.; Sherrell, R. M.; Lambert, C.; Bucciarelli, E.; Sarthou, G.; Le Goff, M.; Liorzou, C.; Chéron, S.; Viollier, E.; Gayet, N. Contribution of resuspended sedimentary particles to dissolved iron and manganese in the ocean: An experimental study. *Chem. Geol.* **2019**, *511*, 389.
- (58) Ingall, E. D.; Diaz, J. M.; Longo, A. F.; Oakes, M.; Finney, L.; Vogt, S.; Lai, B.; Yager, P. L.; Twining, B. S.; Brandes, J. A. Role of biogenic silica in the removal of iron from the Antarctic seas. *Nat. Commun.* **2013**, *4*, 1981.
- (59) Lam, P. J.; Lee, J.-M.; Heller, M. I.; Mehic, S.; Xiang, Y.; Bates, N. R. Size-fractionated distributions of suspended particle concentration and major phase composition from the U.S. GEOTRACES Eastern Pacific Zonal Transect (GP16). *Mar. Chem.* **2018**, 201, 90–107.
- (60) Wagener, T.; Guieu, C.; Leblond, N. Effects of dust deposition on iron cycle in the surface Mediterranean Sea: results from a mesocosm seeding experiment. *Biogeosciences* **2010**, 7 (11), 3769–3781.
- (61) Ye, Y.; Wagener, T.; Volker, C.; Guieu, C.; Wolf-Gladrow, D. A. Dust deposition: iron source or sink? A case study. *Biogeosciences* **2011**, *8* (8), 2107–2124.
- (62) Beghoura, H.; Gorgues, T.; Aumont, O.; Planquette, H. F.; Tagliabue, A.; Auger, P. A. Impact of Inorganic Particles of Sedimentary Origin on Global Dissolved Iron and Phytoplankton Distribution. J. Geophys. Res.: Oceans 2019, 124 (12), 8626–8646.
- (63) Tovar-Sanchez, A.; Sanudo-Wilhelmy, S. A.; Garcia-Vargas, M.; Weaver, R. S.; Popels, L. C.; Hutchins, D. A. A trace metal clean reagent to remove surface-bound iron from marine phytoplankton. *Mar. Chem.* **2003**, 82 (1–2), 91–99.

- (64) Twining, B. S.; Baines, S. B. The Trace Metal Composition of Marine Phytoplankton. *Annual Review of Marine Science* **2013**, *5* (1), 191–215.
- (65) Anderson, R. F. Chemical Tracers of Particle Transport. In *Treatise on Geochemistry*; Elderfield, H., Turekian, K. K., Eds.; Elsevier, 2003; Vol. 6, pp 247–273.
- (66) Biscaye, P. E.; Eittreim, S. L. Suspended particulate loads and transports in the nepheloid layer of the abyssal Atlantic Ocean. *Mar. Geol.* 1977, 23 (1–2), 155–172.
- (67) Tagliabue, A.; Bowie, A. R.; Boyd, P. W.; Buck, K. N.; Johnson, K. S.; Saito, M. A. The integral role of iron in ocean biogeochemistry. *Nature* **2017**, *543* (7643), *51*–59.
- (68) Revsbech, N. P.; Larsen, L. H.; Gundersen, J.; Dalsgaard, T.; Ulloa, O.; Thamdrup, B. Determination of ultra-low oxygen concentrations in oxygen minimum zones by the STOX sensor. *Limnol. Oceanogr.: Methods* **2009**, *7*, 371–381.
- (69) Scholz, F.; Löscher, C. R.; Fiskal, A.; Sommer, S.; Hensen, C.; Lomnitz, U.; Wuttig, K.; Göttlicher, J.; Kossel, E.; Steininger, R.; Canfield, D. E. Nitrate-dependent iron oxidation limits iron transport in anoxic ocean regions. *Earth Planet. Sci. Lett.* **2016**, 454, 272–281.
- (70) Henrichs, S. M.; Farrington, J. W. Peru upwelling region sediments near 15°S. 1. Remineralization and accumulation of organic matter1. *Limnol. Oceanogr.* **1984**, *29* (1), 1–19.
- (71) Hansell, D.; Carlson, C.; Repeta, D.; Schlitzer, R. Dissolved organic matter in the ocean: New insights stimulated by a controversy. *Oceanography* **2009**, 22 (4), 202–211.
- (72) Penven, P.; Echevin, V.; Pasapera, J.; Colas, F.; Tam, J. Average circulation, seasonal cycle, and mesoscale dynamics of the Peru Current System: A modeling approach. *Journal of Geophysical Research: Oceans* **2005**, *110* (C10), 1–21.
- (73) Chaigneau, A.; Pizarro, O. Eddy characteristics in the eastern South Pacific. *Journal of Geophysical Research: Oceans* **2005**, *110* (C6), 1–18.
- (74) Chaigneau, A.; Gizolme, A.; Grados, C. Mesoscale eddies off Peru in altimeter records: Identification algorithms and eddy spatiotemporal patterns. *Prog. Oceanogr.* **2008**, 79 (2), 106–119.
- (75) Czeschel, R.; Stramma, L.; Schwarzkopf, F. U.; Giese, B. S.; Funk, A.; Karstensen, J. Middepth circulation of the eastern tropical South Pacific and its link to the oxygen minimum zone. *J. Geophys. Res.* **2011**, *116* (C1), C01015.
- (76) Conway, T. M.; Palter, J. B.; de Souza, G. F. Gulf Stream rings as a source of iron to the North Atlantic subtropical gyre. *Nat. Geosci.* **2018**, *11* (8), 594–598.
- (77) Reinhardt, L.; Kudrass, H.-R.; Lückge, A.; Wiedicke, M.; Wunderlich, J.; Wendt, G. High-resolution sediment echosounding off Peru: Late Quaternary depositional sequences and sedimentary structures of a current-dominated shelf. *Marine Geophysical Researches* **2002**, 23 (4), 335–351.
- (78) Pak, H.; Codispoti, L. A.; Zaneveld, J. R. V. On the intermediate particle maxima associated with oxygen-poor water off western South America. *Deep-Sea Res., Part A* **1980**, 27 (10), 783–797.
- (79) Kim, K. H.; Burnett, W. C. Accumulation and biological mixing of Peru margin sediments. *Mar. Geol.* **1988**, *80* (3), 181–194.
- (80) ATLAS ShakeMap. https://earthquake.usgs.gov/earthquakes/eventpage/usb000jzma/shakemap/intensity (accessed 09/01/2019).
- (81) Cacchione, D. A.; Pratson, L. F.; Ogston, A. S. The Shaping of Continental Slopes by Internal Tides. *Science* **2002**, 296 (5568), 724–727.
- (82) Nash, J.; Kunze, E.; Toole, J.; Schmitt, R. Internal Tide Reflection and Turbulent Mixing on the Continental Slope. *Journal of Physical Oceanography* **2004**, 34 (5), 1117–1134.
- (83) Ribbe, J.; Holloway, P. E. A model of suspended sediment transport by internal tides. *Cont. Shelf Res.* **2001**, 21 (4), 395–422.
- (84) McPhee-Shaw, E. E.; Kunze, E. Boundary layer intrusions from a sloping bottom: A mechanism for generating intermediate nepheloid layers. *Journal of Geophysical Research: Oceans* **2002**, *107* (C6), 3-1–3-16.

- (85) Thorpe, S. A.; White, M. A deep intermediate nepheloid layer. Deep-Sea Res., Part A 1988, 35 (9), 1665–1671.
- (86) Cacchione, D. A.; Drake, D. E. Nepheloid layers and internal waves over continental shelves and slopes. *Geo-Mar. Lett.* **1986**, *6* (3), 147–152.
- (87) McPhee-Shaw, E. E.; Sternberg, R. W.; Mullenbach, B.; Ogston, A. S. Observations of intermediate nepheloid layers on the northern California continental margin. *Cont. Shelf Res.* **2004**, *24* (6), 693–720.
- (88) Mosch, T.; Sommer, S.; Dengler, M.; Noffke, A.; Bohlen, L.; Pfannkuche, O.; Liebetrau, V.; Wallmann, K. Factors influencing the distribution of epibenthic megafauna across the Peruvian oxygen minimum zone. *Deep Sea Res., Part I* **2012**, *68*, 123–135.
- (89) Erdem, Z.; Schönfeld, J.; Glock, N.; Dengler, M.; Mosch, T.; Sommer, S.; Elger, J.; Eisenhauer, A. Peruvian sediments as recorders of an evolving hiatus for the last 22 thousand years. *Quat. Sci. Rev.* **2016**, *137*, 1–14.
- (90) Boyer, T. P.; Antonov, J. I.; Baranova, O. K.; Garcia, H. E.; Johnson, D. R.; Mishonov, A. V.; O'Brien, T. D.; Seidov, D.; Smolyar, I.; Zweng, M. M.; Paver, C. R.; Locarnini, R. A.; Reagan, J. R.; Forgy, C.; Grodsky, A.; Levitus, S., World ocean database 2013; 2013. https://repository.library.noaa.gov/view/noaa/1291.
- (91) Ryan, W. B. F.; Carbotte, S. M.; Coplan, J. O.; O'Hara, S.; Melkonian, A.; Arko, R.; Weissel, R. A.; Ferrini, V.; Goodwillie, A.; Nitsche, F.; Bonczkowski, J.; Zemsky, R. Global Multi-Resolution Topography synthesis. *Geochemistry, Geophysics, Geosystems* **2009**, *10*, 3
- (92) Vu, H. T. D.; Sohrin, Y. Diverse stoichiometry of dissolved trace metals in the Indian Ocean. Sci. Rep. 2013, 3 (1), 1745.
- (93) Noble, A. E.; Lamborg, C. H.; Ohnemus, D. C.; Lam, P. J.; Goepfert, T. J.; Measures, C. I.; Frame, C. H.; Casciotti, K. L.; DiTullio, G. R.; Jennings, J.; Saito, M. A. Basin-scale inputs of cobalt, iron, and manganese from the Benguela-Angola front to the South Atlantic Ocean. *Limnol. Oceanogr.* **2012**, *57* (4), 989–1010.
- (94) Klar, J. K.; Schlosser, C.; Milton, J. A.; Woodward, E. M. S.; Lacan, F.; Parkinson, I. J.; Achterberg, E. P.; James, R. H. Sources of dissolved iron to oxygen minimum zone waters on the Senegalese continental margin in the tropical North Atlantic Ocean: Insights from iron isotopes. *Geochim. Cosmochim. Acta* 2018, 236, 60–78.
- (95) Zheng, L.; Sohrin, Y. Major lithogenic contributions to the distribution and budget of iron in the North Pacific Ocean. *Sci. Rep.* **2019**, 9 (1), 11652.
- (96) Ohnemus, D. C.; Rauschenberg, S.; Cutter, G. A.; Fitzsimmons, J. N.; Sherrell, R. M.; Twining, B. S., Elevated trace metal content of prokaryotic communities associated with marine oxygen deficient zones. *Limnol. Oceanogr.* **2017**, *62* (1), 3–25.
- (97) Cutter, G. A.; Bruland, K. W. Rapid and noncontaminating sampling system for trace elements in global ocean surveys. *Limnol. Oceanogr.: Methods* **2012**, *10*, 425–436.
- (98) Cutter, G. A.; Andersson, P.; Codispoti, L.; Croot, P.; Francois, F.; Lohan, M. C.; Obata, H.; Rutgers van der Loeff, M. Sampling and Sample-handling Protocols for GEOTRACES Cruises, v3.0. https://www.geotraces.org/methods-cookbook/. Accessed June 12, 2020.
- (99) Schlitzer, R. Ocean Data View; 2018. https://odv.awi.de/(Accessed June 12, 2020).
- (100) Gruber, N.; Sarmiento, J. L. Global patterns of marine nitrogen fixation and denitrification. *Global Biogeochemical Cycles* 1997, 11 (2), 235–266.
- (101) Sarmiento, J. L.; Gruber, N.; Brzezinski, M. A.; Dunne, J. P. High-latitude controls of thermocline nutrients and low latitude biological productivity. *Nature* **2004**, 427 (6969), 56–60.
- (102) Bohlen, L.; Dale, A. W.; Sommer, S.; Mosch, T.; Hensen, C.; Noffke, A.; Scholz, F.; Wallmann, K. Benthic nitrogen cycling traversing the Peruvian oxygen minimum zone. *Geochim. Cosmochim. Acta* 2011, 75 (20), 6094–6111.